iScience

CellPress
OPEN ACCESS

Article

Proteome and ubiquitinome analyses of the brain cortex in K18-*hACE2* mice infected with SARS-CoV-2

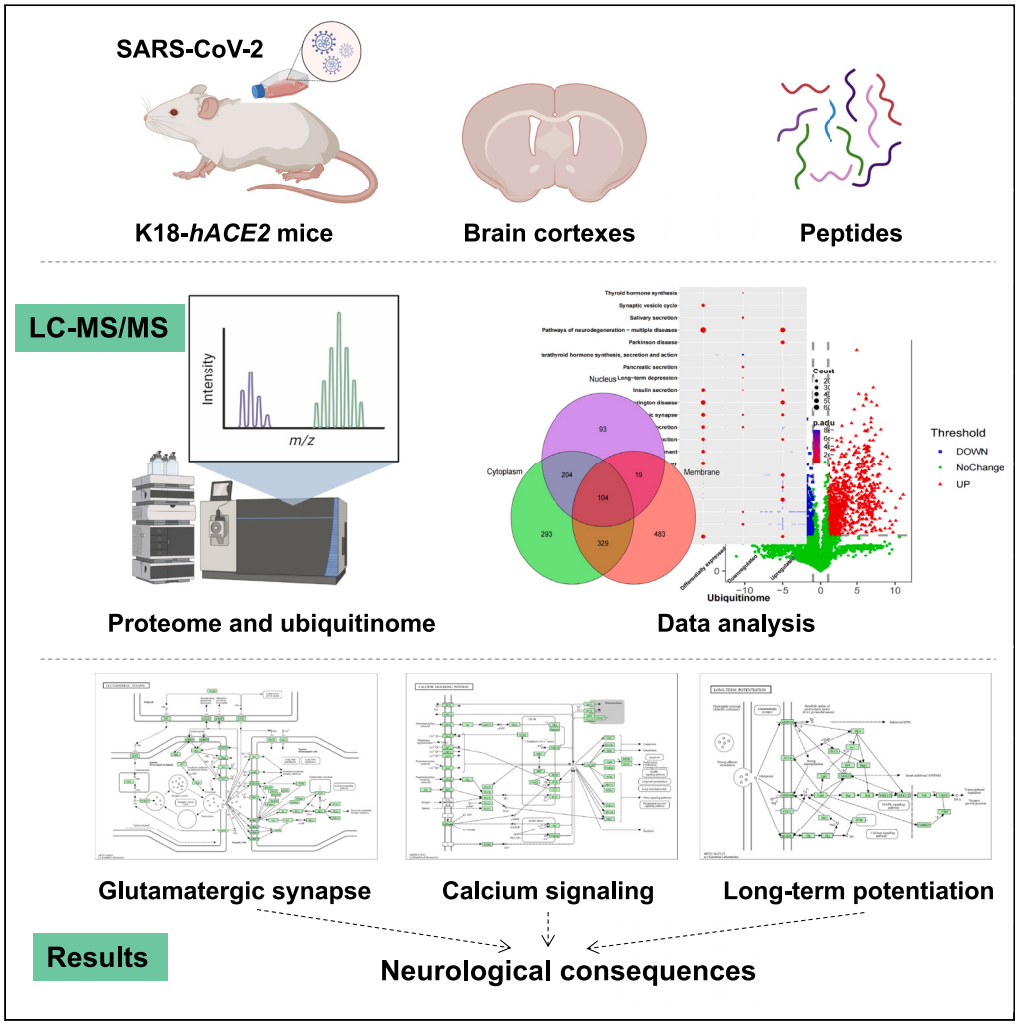

Qiaochu Wang, Wanjun Peng, Yehong Yang, ..., Jiangning Liu, Juntao Yang, Jiangfeng Liu

liujn@cnilas.org (J.L.)
yangjt@pumc.edu.cn (J.Y.)
ljf@pumc.edu.cn (J.L.)

Highlights

This is the first report of the brain cortex ubiquitinome in K18-*hACE2* mice

SARS-CoV-2 may lead to neurological consequences via the glutamatergic synapse pathway

SARS-CoV-2 proteins may interact with host proteins and ubiquitinated sites

Some E3 ubiquitin ligases/deubiquitinases may interact with host ubiquitinated proteins

Wang et al., iScience 27, 110602
September 20, 2024
https://doi.org/10.1016/j.isci.2024.110602

iScience

CellPress
OPEN ACCESS

Article

Proteome and ubiquitinome analyses of the brain cortex in K18-*hACE2* mice infected with SARS-CoV-2

Qiaochu Wang,[1,3] Wanjun Peng,[2,3] Yehong Yang,[1] Yue Wu,[1] Rong Han,[1] Tao Ding,[1] Xutong Zhang,[1] Jiangning Liu,[2,*] Juntao Yang,[1,4,*] and Jiangfeng Liu[1,*]

SUMMARY

Clinical research indicates that SARS-CoV-2 infection is linked to several neurological consequences, and the virus is still spreading despite the availability of vaccinations and antiviral medications. To determine how hosts respond to SARS-CoV-2 infection, we employed LC-MS/MS to perform ubiquitinome and proteome analyses of the brain cortexes from K18-*hACE2* mice in the presence and absence of SARS-CoV-2 infection. A total of 8,024 quantifiable proteins and 5,220 quantifiable lysine ubiquitination (Kub) sites in 2023 proteins were found. Glutamatergic synapse, calcium signaling pathway, and long-term potentiation may all play roles in the neurological consequences of SARS-CoV-2 infection. Then, we observed possible interactions between 26 SARS-CoV-2 proteins/E3 ubiquitin-protein ligases/deubiquitinases and several differentially expressed mouse proteins or Kub sites. We present the first description of the brain cortex ubiquitinome in K18-*hACE2* mice, laying the groundwork for further investigation into the pathogenic processes and treatment options for neurological dysfunction following SARS-CoV-2 infection.

INTRODUCTION

With more than 760 million confirmed cases worldwide, the coronavirus disease 2019 (COVID-19) pandemic caused by severe acute respiratory syndrome coronavirus 2 (SARS-CoV-2) has continued since December 2019.[1] COVID-19 not only affects the respiratory system but also may harm other organs.[2] Among its effects, neurological consequences have emerged as critical issues that cannot be overlooked. SARS-CoV-2 may directly induce neurological damage or indirectly induce neurological damage through cytokine storms or other processes, resulting in symptoms, such as olfactory and taste problems, neurodegenerative illnesses, neuropsychiatric disorders, encephalitis, ischemic stroke, and hemorrhagic stroke.[3] Exploring the mechanisms of neurological damage in patients infected with SARS-CoV-2 will thus aid in improving patient prognosis by enhancing the treatment of these associated problems, minimizing neurological damage, and preventing potential sequelae.

Ubiquitination is a common posttranslational modification (PTM). Ubiquitin is a 76-amino acid-residue protein that consists of seven lysine residues (K6, K11, K27, K29, K33, K48, and K63) that can bind to substrate proteins via three types of enzymes: activating (E1), conjugating (E2), and ligating (E3) enzymes. Its specificity is mainly determined by E3 ubiquitin-protein ligases.[4] Ubiquitin connects to its substrate proteins via the C-terminus, which forms isopeptide bonds with amino groups of residues with lysine in other proteins. Deubiquitinases (DUBs) reverse the ubiquitination of proteins and affect several kinds of biological activities, such as protein degradation, transcription, signaling, and the cell cycle. Factors that cause the dysregulation of E3 ubiquitin-protein ligases or DUBs can initiate the abnormal activation or inactivation of pathways involved in the initiation and development of numerous disorders, especially tumors and neurological diseases.[5–8] The results of distribution and bioinformatics analyses of the global ubiquitinated proteomes in the cerebral cortexes of normal humans and mice have been reported and compared with those of several disease models to analyze the role of ubiquitination in disease.[9–17] However, only the ubiquitinomes of Vero E6 cells and human lung epithelial cell lines infected with SARS-CoV-2 have been reported, and the changes in ubiquitination modifications and possible pathogenic mechanisms in brain cortexes infected with SARS-CoV-2 are not known.

We explored the ubiquitinome and proteome in the cortex of K18-*hACE2* mice infected or not infected with SARS-CoV-2 and studied the differences between the SARS-CoV-2 infection group and the control group to examine the relationship between the neurological consequences of COVID-19 and ubiquitination in the brain cortex. To some extent, K18-*hACE2* mice may imitate the respiratory and neurological

[1]State Key Laboratory of Common Mechanism Research for Major Diseases, Department of Biochemistry and Molecular Biology, Institute of Basic Medical Sciences, Chinese Academy of Medical Sciences & Peking Union Medical College, Beijing 100005, China
[2]NHC Key Laboratory of Human Disease Comparative Medicine, Beijing Key Laboratory for Animal Models of Emerging and Remerging Infectious Diseases, Institute of Laboratory Animal Science, CAMS and Comparative Medicine Center, Peking Union Medical College, Beijing 100021, China
[3]These authors contributed equally
[4]Lead contact
*Correspondence: liujn@cnilas.org (J.L.), yangjt@pumc.edu.cn (J.Y.), ljf@pumc.edu.cn (J.L.)
https://doi.org/10.1016/j.isci.2024.110602

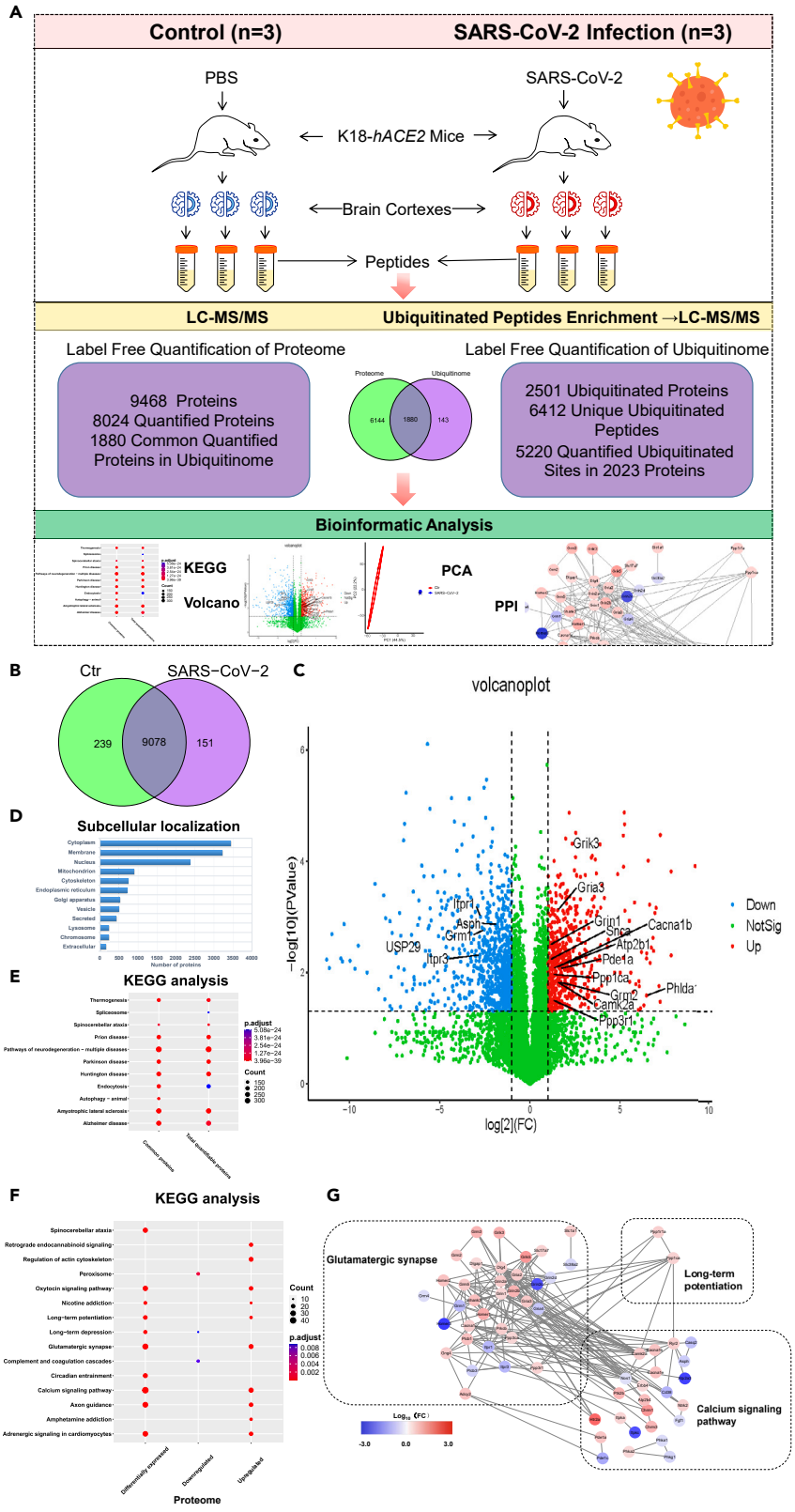
A
Control (n=3)
SARS-CoV-2 Infection (n=3)
PBS
SARS-CoV-2
K18-hACE2 Mice
Brain Cortexes
Peptides
LC-MS/MS
Ubiquitinated Peptides Enrichment →LC-MS/MS
Label Free Quantification of Proteome
Label Free Quantification of Ubiquitinome
9468 Proteins
8024 Quantified Proteins
1880 Common Quantified Proteins in Ubiquitinome
Proteome
Ubiquitinome
6144
1880
143
2501 Ubiquitinated Proteins
6412 Unique Ubiquitinated Peptides
5220 Quantified Ubiquitinated Sites in 2023 Proteins
Bioinformatic Analysis
KEGG
Volcano
PCA
PPI
B
Ctr
SARS−CoV−2
239
9078
151
C
volcanoplot
−log[10](PValue)
log[2](FC)
Down
NotSig
Up
Grik3
Gria3
Grin1
Cacna1b
Snca
Atp2b1
Pde1a
Ppp1ca
Camk2a
Ppp3r1
Phlda
Itpr1
Asph
Grm1
USP29
Itpr3
D
Subcellular localization
Cytoplasm
Membrane
Nucleus
Mitochondrion
Cytoskeleton
Endoplasmic reticulum
Golgi apparatus
Vesicle
Secreted
Lysosome
Chromosome
Extracellular
Number of proteins
E
KEGG analysis
Thermogenesis
Spliceosome
Spinocerebellar ataxia
Prion disease
Pathways of neurodegeneration − multiple diseases
Parkinson disease
Huntington disease
Endocytosis
Autophagy − animal
Amyotrophic lateral sclerosis
Alzheimer disease
p.adjust
Count
Quantified proteins
Total identifiable proteins
F
KEGG analysis
Spinocerebellar ataxia
Retrograde endocannabinoid signaling
Regulation of actin cytoskeleton
Peroxisome
Oxytocin signaling pathway
Nicotine addiction
Long−term potentiation
Long−term depression
Glutamatergic synapse
Complement and coagulation cascades
Circadian entrainment
Calcium signaling pathway
Axon guidance
Amphetamine addiction
Adrenergic signaling in cardiomyocytes
Differentially expressed
Downregulated
Upregulated
Proteome
G
Glutamatergic synapse
Long-term potentiation
Calcium signaling pathway
Count
p.adjust

Figure 1. Bioinformatics analysis and proteomics analysis of the brain cortex

(A) Workflow for the K18-hACE2 mouse brain cortex proteome and ubiquitinome analyses.

(B) Venn diagram of the identified proteins.

(C) Volcano plot displaying the log_2FC values of the differentially expressed quantifiable proteins in the SARS-CoV-2 infection group versus the control group (FC > 2 or <0.5; t test, significance; *p* value < 0.05). The red dots represent the 601 significantly upregulated quantifiable proteins, and the blue dots represent the 774 downregulated quantifiable proteins.

(D) Subcellular localization of the quantifiable proteins.

(E) The top 10 enriched terms in the KEGG pathway enrichment analysis of total quantifiable proteins and common proteins.

(F) The top 10 enriched terms identified through KEGG analysis of upregulated proteins, downregulated proteins, and all differentially expressed proteins (including upregulated and downregulated proteins).

(G) PPI networks of differentially expressed proteins enriched in KEGG pathways ("glutamatergic synapse", "long-term potentiation", and "calcium signaling pathway") with a confidence score ≥ 0.7. If a protein was present in two or more pathways according to the KEGG analysis, only the pathway with the lowest *p* value was included in the PPI network.

symptoms of COVID-19 patients after SARS-CoV-2 infection, and SARS-CoV-2 RNA and antigens can also be detected in the brains of these mice. In summary, K18-*hACE2* mice encapsulate many of the characteristics found in COVID-19 patients and serve as a viable model for researching the pathophysiology of and assessing COVID-19 interventions.[18–20] This research included *in vivo* observations as well as data on COVID-19 mechanisms and potential therapeutic targets.

RESULTS

Brain cortex proteomic study in SARS-CoV-2-infected K18-*hACE2* mice

We evaluated the brain cortexes of three mock-infected K18-*hACE2* mice and three infected K18-*hACE2* mice (control and SARS-CoV-2 infection groups, *n* = 3 per group) and performed label-free quantitative analyses of the proteome and ubiquitinome (Figure 1A). The SARS-CoV-2 nucleic acid load test findings (Figure S1) revealed that the three infected mouse brain cortexes exhibited similar viral loads. Our proteomics data from the control and SARS-CoV-2 infection groups revealed 9,468 distinct proteins, 8,024 of which were quantifiable, while the ubiquitinomics data revealed 5,220 quantifiable Kub sites in 2,023 proteins, 89% (1,880) of which overlapped with the quantifiable proteins identified in the proteomic analysis (Figure 1A). Most of the quantifiable proteins were found in both the control and SARS-CoV-2 infection groups (Figure 1B). Based on a fold change (FC) greater than 2 or less than 0.5 and a t test *p* value less than 0.05 as the criterion for significance, 601 proteins were upregulated and 774 were downregulated (Figure 1C and Table S1). According to our bioinformatics analysis, the quantifiable proteins were distributed mainly in the cytoplasm, membrane, nucleus, and mitochondria (Figure 1D). There was significant overlap among these key biological components since many proteins were distributed in numerous compartments. The Kyoto Encyclopedia of Genes and Genomes (KEGG) pathway enrichment analysis demonstrated that overall, quantifiable proteins were enriched in "pathways of neurodegeneration-multiple diseases", "thermogenesis", "spliceosome", and "endocytosis", which are very similar to those of common proteins (Figure 1E and Table S2). To evaluate the quality of the MS data, we constructed a number of plots, including a principal component analysis (PCA) plot (Figures S2A–S2F).

Proteomic functional alterations in the brain cortex of K18-*hACE2* mice following SARS-CoV-2 infection

KEGG analysis revealed that the upregulated proteins were more enriched in the "glutamatergic synapse" pathway, "calcium signaling" pathway, pathways involved in "nicotine addiction", "oxytocin signaling" pathway, and other pathways. However, the downregulated proteins were enriched in the "peroxisome" signaling, "complement and coagulation cascades", and "long-term depression" (Figure 1F and Tables S3 and S4). For all the differentially expressed proteins, the top three pathways identified via KEGG analysis were the "glutamatergic synapse" pathway, "calcium signaling" pathway and "long-term potentiation" pathway (Figure 1F and Table S5). In the "glutamatergic synapse" pathway, there were several upregulated glutamate receptors (Grin1, Grm2, Gria3, Grik3, etc.) and several downregulated proteins (Itpr1, Itpr3, Grm1, etc.). In the "calcium signaling pathway", many calcium regulation-associated proteins exhibited altered expression (Atp2b1, Pde1a, Cacna1b, Camk2a, etc.). The protein phosphatases Ppp3r1 and Ppp1ca were upregulated in "long-term potentiation" pathway, which may regulate cognitive function by dephosphorylating a large number of proteins (Figure 1G and Table S6). Notably, the expression of alpha-synuclein (SNCA) was significantly upregulated after SARS-CoV-2 infection. SNCA is located in the presynaptic cytoplasm of the central nervous system and is a major component of Lewy bodies and Lewy ganglia. Moreover, it is one of the most abundant proteins found in the nervous system, comprising approximately 1% of all nervous system cytoplasmic proteins that regulate the vesicular transport of synaptic neurotransmitters. Its overexpression and aggregation are the main pathological features of Parkinson's disease. Parkinson's disease is a primary neurodegenerative disease of major concern today that is mainly characterized by movement disorders.[21] The upregulation of SNCA corroborates the findings of a previous study reporting increased morbidity and mortality in Parkinson's disease patients following SARS-CoV-2 infection.[3]

Ubiquitinome analysis of the brain cortex in SARS-CoV-2-infected K18-*hACE2* mice

A Venn diagram was constructed to summarize the common and unique elements between the ubiquitinomes of the control group and the SARS-CoV-2 infection group (Figures 2A–2C). In the ubiquitinomes of the control and SARS-CoV-2 infection groups, we identified 6,269 Kub sites and 6,412 unique Kub peptides in 2,501 proteins, 5,220 Kub sites of which were quantifiable (908 significantly upregulated (FC > 2 and t

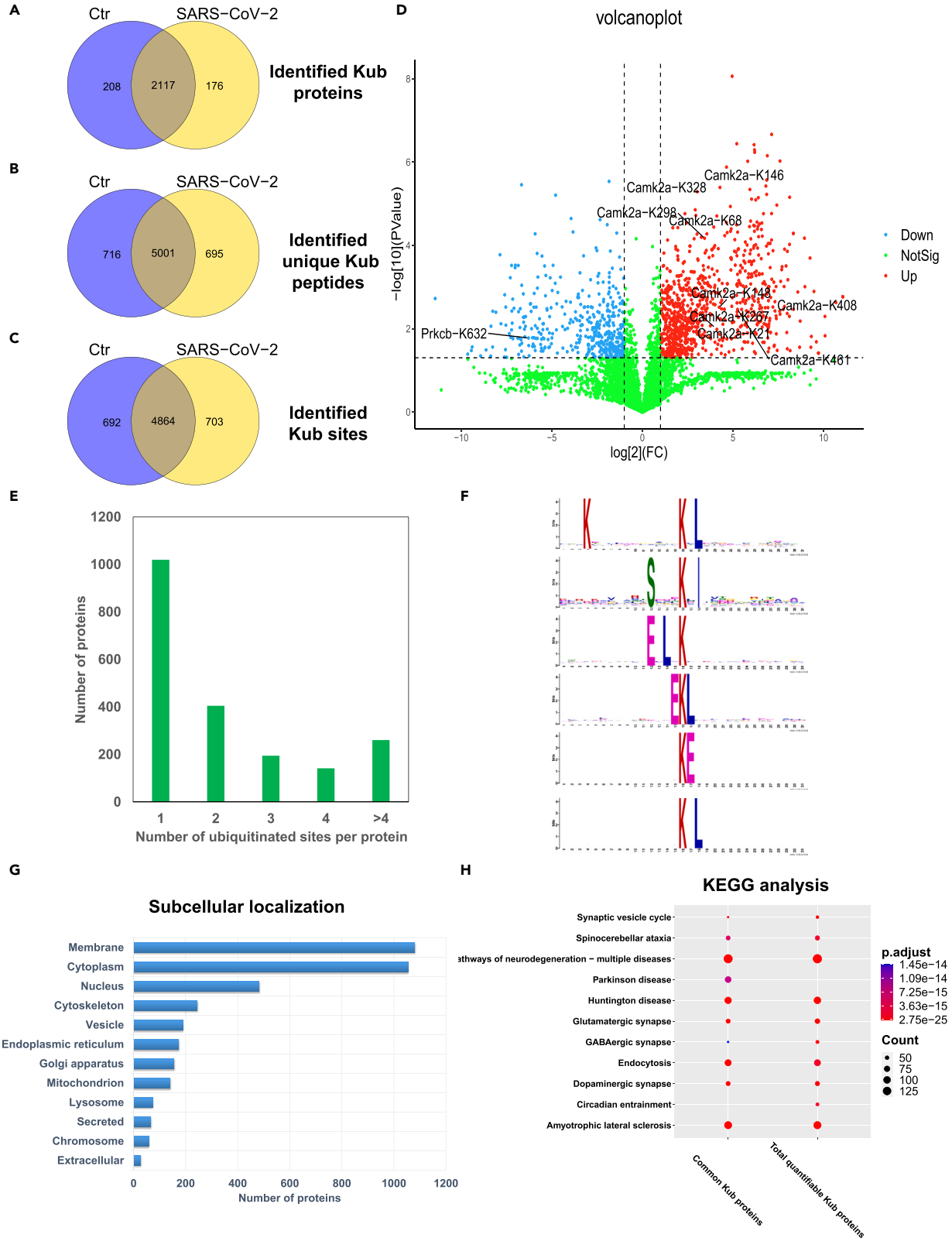
A
Ctr
SARS−CoV−2
208
2117
176
Identified Kub proteins
B
Ctr
SARS−CoV−2
716
5001
695
Identified unique Kub peptides
C
Ctr
SARS−CoV−2
692
4864
703
Identified Kub sites
D
volcanoplot
−log[10](PValue)
log[2](FC)
Camk2a−K146
Camk2a−K328
Camk2a−K298
Camk2a−K68
Camk2a−K148
Camk2a−K408
Camk2a−K267
Camk2a−K21
Camk2a−K461
Prkcb−K632
Down
NotSig
Up
E
Number of proteins
Number of ubiquitinated sites per protein
F
G
Subcellular localization
Membrane
Cytoplasm
Nucleus
Cytoskeleton
Vesicle
Endoplasmic reticulum
Golgi apparatus
Mitochondrion
Lysosome
Secreted
Chromosome
Extracellular
Number of proteins
H
KEGG analysis
Synaptic vesicle cycle
Spinocerebellar ataxia
Parkinson disease
Huntington disease
Glutamatergic synapse
GABAergic synapse
Endocytosis
Dopaminergic synapse
Circadian entrainment
Amyotrophic lateral sclerosis
Common Kub proteins
Total quantifiable Kub proteins
p.adjust
Count

Figure 2. Overview of ubiquitinomics analysis of the brain cortex

(A–C) Venn diagrams of (A) identified Kub proteins, (B) identified unique Kub peptides, and (C) identified Kub sites in the two groups.

(D) Volcano plot displaying the log_2FC values of quantifiable Kub site intensities in the SARS-CoV-2 infection group versus the control group (FC > 2 or <0.5; t test, significance; p value < 0.05). The red dots represent 908 significantly upregulated quantifiable Kub sites in 485 proteins, and the blue dots represent the 446 downregulated quantifiable Kub sites in 308 proteins.

(E) Number of quantifiable Kub sites per protein.

(F) Sequence logo of 31-mer Kub motifs with high scores (+/−15 amino acids from the targeted lysine residue). The motifs were identified using all Kub peptides containing quantifiable Kub sites.

(G) Subcellular localization of quantifiable Kub proteins.

(H) The top 10 enriched terms in the KEGG pathway enrichment analysis of total quantifiable Kub proteins and common Kub proteins.

test p value < 0.05) Kub sites in 485 proteins and 446 downregulated (FC < 0.5 and t test p value < 0.05) Kub sites in 308 proteins) (Figures 1A, 2D, and S3A and Table S7). Approximately half of the proteins had only one Kub site (Figure 2E). To validate the quality of the ubiquitinome MS data, we constructed a number of plots, such as a PCA plot, an Andromeda score distribution plot, a scatterplot with the density in mass inaccuracy displayed by color, a classification plot based on localization probability, a scatterplot, and a density distribution plot, which suggested that the MS data were reliable. After that, we evaluated 5,220 sequences surrounding the quantifiable Kub sites and selected the six highest-scoring motifs. According to the findings, glutamic acid (E) was the most common amino acid upstream of the Kub site, whereas leucine (L) was the most frequently occurring amino acid downstream of the Kub site.

We subsequently conducted a subcellular localization analysis of quantifiable Kub proteins, which were mostly located in the membrane, cytoplasm, nucleus, and cytoskeleton (Figure 2G). KEGG analysis was also conducted for quantifiable Kub proteins to determine the associated metabolic and human disease pathways. We discovered that the most enriched pathways associated with the quantifiable Kub proteins were the "glutamatergic synapse" pathway, "pathways of neurodegeneration—multiple diseases", and "synaptic vesicle cycle" pathway, which are very similar to those of common Kub proteins (Figure 2H and Table S8). In contrast to other Kub proteins found in noncortical cell lines after infection with SARS-CoV-2, our study identified several new Kub proteins enriched in specific KEGG pathways, such as the "glutamatergic synapse" pathway, which shows that the types of Kub proteins differ depending on the organ and species and participate in specific pathways (Figures S4A–S4F and Table S9).[2,22,23]

Functional annotation of proteins with differential ubiquitination in the brain cortex of K18-*hACE2* mice following SARS-CoV-2 infection

KEGG analysis revealed that both the proteins with upregulated ubiquitination and the proteins with downregulated ubiquitination were enriched in the "glutamatergic synapse" pathway and "insulin secretion", respectively. However, the proteins with upregulated ubiquitination were specifically enriched in "pathways of neurodegeneration—multiple diseases", "Huntington disease", and "Parkinson disease", whereas the proteins with downregulated ubiquitination were expressly enriched in pathways of secretion, such as "gastric acid secretion", "pancreatic secretion", "salivary secretion", "aldosterone synthesis and secretion", and "parathyroid hormone synthesis, secretion, and action" (Figure 3A and Tables S10 and S11). For all of the differentially expressed proteins, the first three pathways identified via KEGG analysis were the "glutamatergic synapse" pathway, "insulin secretion", and "gastric acid secretion" (Figures 3A and 3B and Tables S12 and S13). The biological processes of the latter two pathways do not occur in the brain cortex, so we want to rename these two pathways based on the proteins within them. The proteins in the two pathways have a similar function: transmembrane transport. For instance, the calcium-activated potassium channel subunit alpha-1 (Kcnma1) can mediate the export of K^+. Its upregulation may dampen the excitatory events that elevate the cytosolic Ca^{2+} concentration and depolarize the cell membrane, thereby regulating transmitter release and innate immunity.[24] Itpr1 is an intracellular channel protein that mediates calcium release from the endoplasmic reticulum following stimulation by inositol 1,4,5-trisphosphate.[25] Slc4a2 is a sodium-independent anion exchanger that regulates the electroneutral exchange of chloride for bicarbonate ions across the cell membrane.[26] Rab3a is a small GTP-binding protein that controls the recruitment, tethering, and docking of secretory vesicles to the plasma membrane.[27] Vesicle-associated membrane protein Vamp8 is involved in the targeting and fusion of transport vesicles to their target membrane.[28] Therefore, we have renamed these two pathways as the "transmembrane transport" pathway, in which SARS-CoV-2 infection affects the transport of various substances inside and outside the cell, especially neurotransmitters, by altering protein ubiquitination, thus affecting brain function.

Most of the Kub site changes were consistent with the trends in protein changes following SARS-CoV-2 infection, such as the alterations in Grin1, Adcy2, Camk2a, Camk2b, Camk2d, and Camk2g. There were only a few proteins with the opposite trends at the Kub site, including Gja1, Ankrd13a, Prxl2a, Epb41, Prkcb, Syp, and Large1. These findings may indicate that most ubiquitination modifications regulate substrate proteins independently of proteasomal degradation (Figure 3C). Among these several proteins, peroxiredoxin-like 2A (Prxl2a) may inhibit the production of inflammatory cytokines by macrophages through MAPK signaling pathway inhibition.[29] SARS-CoV-2 infection may degrade this protein by upregulating its Kub site, leading to the increased production of inflammatory factors by macrophages, which in turn triggers a cytokine storm that damages the central nervous system.[3] The protein kinase C beta type (Prkcb; an upregulated protein with downregulated Kub sites) controls the activity of downstream proteins by phosphorylating downstream protein serine/threonine residues and plays important roles in multiple pathways, including the "glutamatergic synapse" pathway, "calcium signaling" pathway, "long-term potentiation", and secretion pathways.[30] Synaptophysin (Syp; an upregulated protein with downregulated Kub sites) is involved in the regulation of short- and long-term synaptic plasticity.[31]

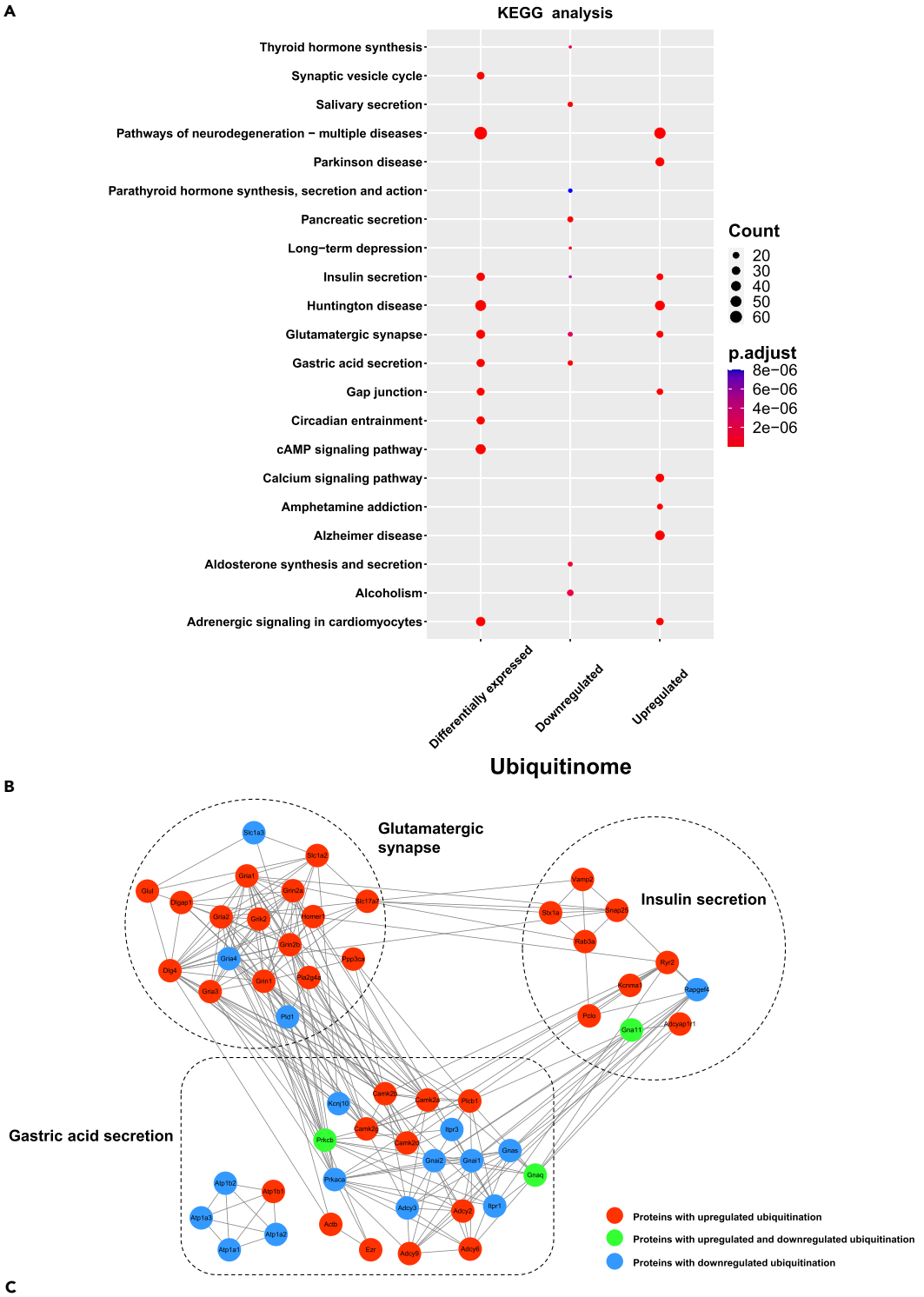
A
KEGG analysis
Thyroid hormone synthesis
Synaptic vesicle cycle
Salivary secretion
Pathways of neurodegeneration − multiple diseases
Parkinson disease
Parathyroid hormone synthesis, secretion and action
Pancreatic secretion
Long−term depression
Insulin secretion
Huntington disease
Glutamatergic synapse
Gastric acid secretion
Gap junction
Circadian entrainment
cAMP signaling pathway
Calcium signaling pathway
Amphetamine addiction
Alzheimer disease
Aldosterone synthesis and secretion
Alcoholism
Adrenergic signaling in cardiomyocytes
Differentially expressed
Downregulated
Upregulated
Count
20
30
40
50
60
p.adjust
8e−06
6e−06
4e−06
2e−06
B
Ubiquitinome
Glutamatergic synapse
Insulin secretion
Gastric acid secretion
Proteins with upregulated ubiquitination
Proteins with upregulated and downregulated ubiquitination
Proteins with downregulated ubiquitination
C
Ubiquitinome
Proteome
Gja1
Epb41
Ankrd13a
Prxl2a
Prkcb
Syp
Large1
Up
Down

Figure 3. Comparison of the label-free ubiquitinomes in the control and SARS-CoV-2 infection groups

(A) The top 10 enriched terms identified through KEGG analysis of proteins with upregulated ubiquitination, proteins with downregulated ubiquitination, and proteins with differentially expressed ubiquitination.

(B) PPI networks of differentially expressed Kub proteins in enriched KEGG pathways ("glutamatergic synapse", "insulin secretion" and "gastric acid secretion") with a confidence score ≥ 0.7. The red circles represent proteins with upregulated ubiquitination, the blue circles represent proteins with downregulated ubiquitination, and the green circles represent proteins with both upregulated and downregulated ubiquitination. If a protein was present in two or more pathways according to the KEGG analysis, only the pathway with the lowest *p* value was included in the PPI network.

(C) Proteins with opposite changes in ubiquitination sites and protein expression.

SARS-CoV-2 viral protein-host protein and Kub site interactions in the brain cortexes of K18-*hACE2* mice

SARS-CoV-2 encodes four basic proteins, membrane protein (M), envelope protein (E), spike protein (S), and nucleocapsid phosphoprotein (N), sixteen nonstructural proteins (nsps), and nine accessory proteins.[32] According to a previous study on the interactions between SARS-CoV-2 particles and human proteins,[33] we matched differentially expressed proteins and Kub sites in mice to those in humans by BLAST and constructed networks among SARS-CoV-2 proteins and mouse proteins in this study (Figure 4 and Table S14). We identified 26 SARS-CoV-2 proteins that may interact with 92 host proteins containing 117 Kub sites with altered expression. Several of the proteins were associated the "glutamatergic synapse" pathway, "calcium signaling" pathway, "long-term potentiation", and secretion pathways, such as Itp1 (a downregulated protein with downregulated Kub sites), Itp3 (a downregulated protein with downregulated Kub sites), Gnai1 (a protein with downregulated Kub sites), and Asph (a downregulated protein). In summary, these viral proteins interact with a range of differentially expressed proteins and Kub sites and may be drug targets for treating SARS-CoV-2 infection.

Finally, we combined the differentially expressed proteins and Kub sites in highly enriched pathways (the "glutamatergic synapse" pathway, "calcium signaling" pathway, and "long-term potentiation") in cellular and subcellular diagrams to provide additional comprehensive and comprehensible data regarding the functional modifications following SARS-CoV-2 infection (Figure 5 and Table S15).

Experimental verification

To verify the reliability of the mass spectrometry results, we performed immunohistochemical experiments on ubiquitin carboxyl-terminal hydrolase 29 (Usp29) and pleckstrin homology-like domain family A member 1 (Phlda1). The DUB Usp29 is a downregulated protein in the mouse brain cortex that can promote cellular anti-DNA-related viral responses and autoimmunity.[34] However, previous studies have reported that Usp29 can enhance SARS-CoV-2 virulence by preventing the proteasomal degradation of ORF9b, and the level of the USP29 mRNA in the peripheral blood mononuclear cells of SARS-CoV-2 patients was higher than that in healthy individuals.[35] Interestingly, the change in the USP mRNA levels in human peripheral blood mononuclear cells did not correspond with those in the USP protein levels in the mouse cerebral cortexes. This may be due to problems with protein degradation or translation processes or differences in tissue type. Phlda1 was one of the most upregulated proteins in the infected mice. Phlda1 belongs to the PHLDA family and can induce neuronal cell pyroptosis in rats.[36] Its upregulation may be an important cause of neurological sequelae. As determined by immunohistochemical staining, the changes in the levels of these two proteins were consistent with the mass spectrometry results, which confirmed the reliability of our experiment (Figure 6).

DISCUSSION

In this study, we investigated the proteomes and ubiquitinomes of the brain cortexes of control and SARS-CoV-2-infected K18-*hACE2* mice and identified the "glutamatergic synapse" pathway, "calcium signaling" pathway, and "long-term potentiation" as enriched pathways. These findings are complementary to other proteomic studies and could prove the reliability of other findings and complement new post-infection proteins. All three brain tissues showed considerable increases in SNCA expression levels following infection. We still evaluated the viral proteins even if they were not ubiquitinated. This study provides a brain proteomics and ubiquitinomics dataset from mice infected SARS-CoV-2, as well as the involved pathways and responses that occur in the cortex in response to SARS-CoV-2 infection in K18-*hACE2* mice.

SARS-CoV-2 infection induces insomnia, weariness, cognitive impairment, Parkinson's disease, Alzheimer's disease, and anxiety in addition to the previously stated olfactory and taste problems.[37] Glutamate is the most abundant excitatory neurotransmitter in the mammalian brain and is packaged into synaptic vesicles at the presynaptic terminal. When glutamate is released into the synaptic cleft, it either acts on postsynaptic ionotropic glutamate receptors to mediate rapid excitatory synaptic transmission or on postsynaptic metabotropic glutamate receptors to exert several regulatory effects through the coupling of these receptors to G proteins and subsequent recruitment of second messenger systems.[38] It has been proposed that cognitive impairment in SARS-CoV-2 infection may be caused by glutamatergic dysfunction.

Some studies about COVID-19 suggest that neurological sequelae are caused by blood-brain barrier breakdown and systemic inflammation,[39–43] which unfortunately is not well represented in the cerebral cortex of mice in our study. This may be due to differences in the type of tissues and the sampling time of brain tissue. However, our finding that the glutaminergic synaptic pathway may cause neurological sequelae is also consistent with the conclusions of other studies.[44–46] And some important protein changes are the same in mice brain and human brain,[43,47] such as the ubiquitin-like protein ISG15, the postsynaptic protein syntaxin-1A, homer protein homolog 1, the fibronectin leucine-rich transmembrane protein-3, the ubiquitin-associated and SH3 domain-containing protein B and so on, which play important roles in inflammatory response and synaptic homeostasis.

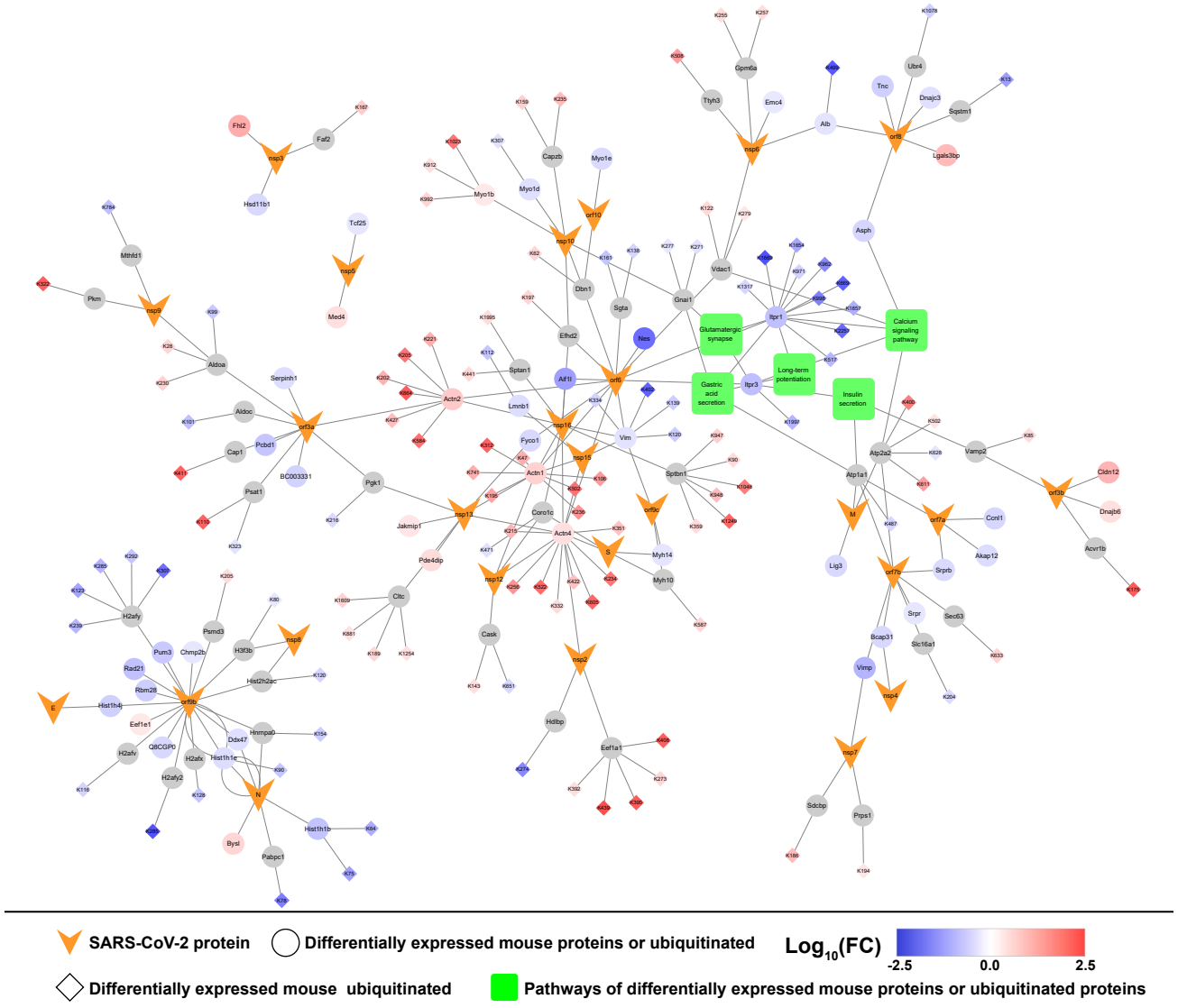

Figure 4. PPI networks of SARS-CoV-2 viral proteins, differentially expressed proteins, and differentially expressed Kub sites based on the reported SARS-CoV-2 protein interactome

The orange arrows represent viral proteins, the circles represent differentially expressed mouse proteins or proteins with differentially expressed Kub sites, and the diamonds represent differentially expressed mouse Kub sites. The colors of the circles or diamonds represent the abundance of proteins/Kub sites in the brain cortexes; the gray circles represent constantly expressed proteins with differentially expressed Kub sites; and the green boxes represent Kyoto Encyclopedia of Genes and Genomes (KEGG) enrichment pathways of the linked proteins.

Parkinson's disease is one of several disorders called synuclein disease that result from the misfolding and aggregation of SNCA(an unregulated protein).[48] Parkinson's syndrome is a clinical syndrome characterized by quiescence tremor, bradykinesia, muscle stiffness, postural instability, gait disturbance, cognitive impairment, decreased sense of smell, anxiety, and depression.[49–52] In a mouse model of Parkinson's disease in which SNCA is overexpressed in the brain, increased glutaminergic signaling may be the molecular mechanism for the exacerbation of clinical symptoms.[53] Besides, Alzheimer's disease is a degenerative disease of the central nervous system characterized by the accumulation of extracellular amyloid protein and intracellular neurofibrillary tangles, with clinical manifestations such as memory impairment, aphasia, apraxia, and agnosia. In Alzheimer's disease, reduced glutamate uptake caused by amyloid protein is an important mechanism of neuronal swelling and even cell death, so the glutaminergic system is one of its important therapeutic targets.[54] These results are similar to our conjecture: "glutamatergic synapse" pathway is critical in the neurological consequences after SARS-CoV-2 infection.

Furthermore, the "calcium signaling" pathway and "long-term potentiation" are closely related to the "glutamatergic synapse" pathway, and several proteins are involved in 2 or all 3 of these pathways (Figure 5). For example, the calcium/calmodulin-dependent protein kinase type

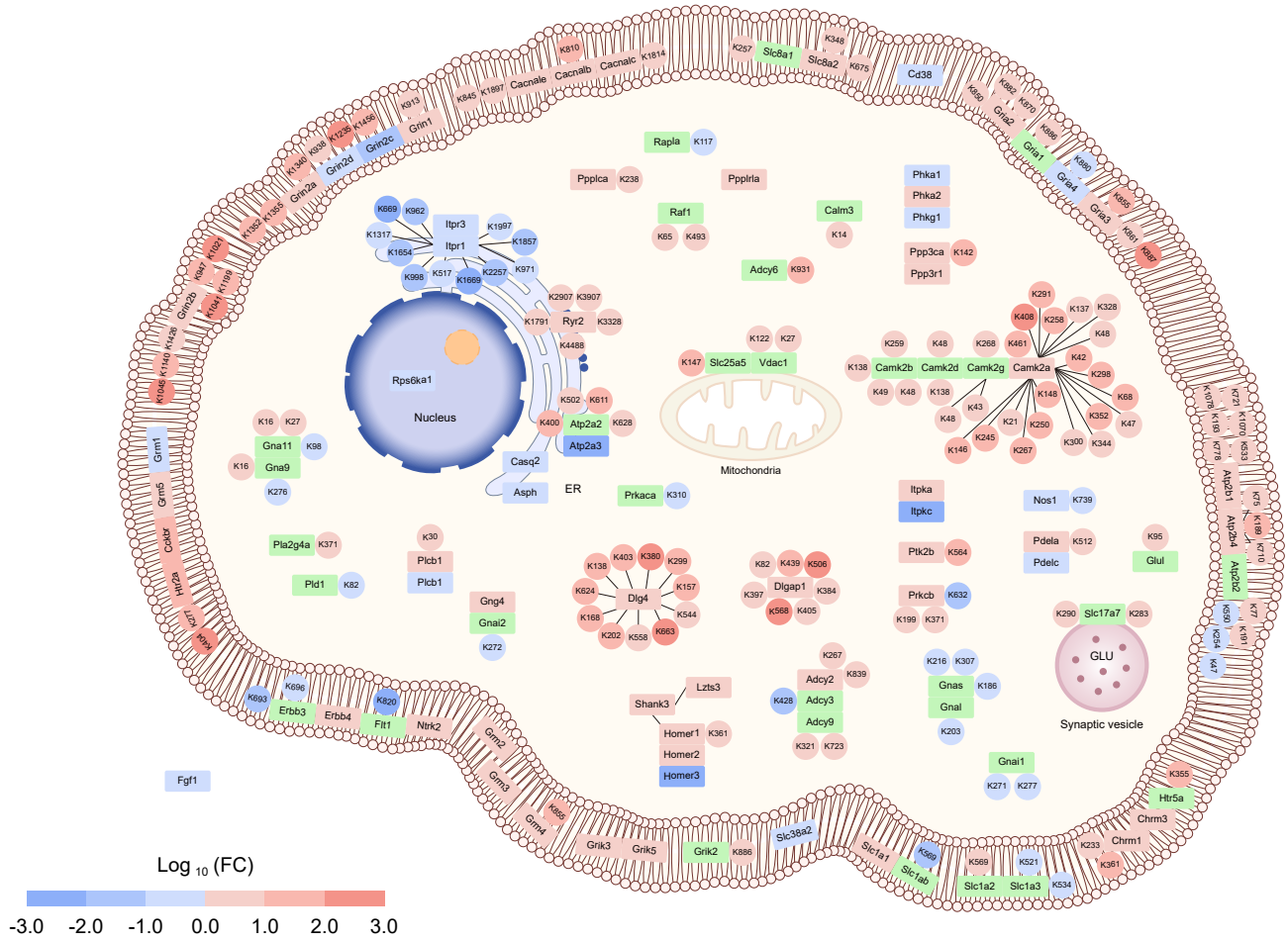

Figure 5. Differentially expressed proteins and differentially expressed Kub sites related to the glutamatergic synapse pathway, long-term potentiation, and the calcium signaling pathway in the brain cortex

The boxes represent differentially expressed proteins. The circles represent differentially expressed Kub sites. The green boxes represent proteins with both constantly expressed proteins and differentially expressed Kub sites.

II proteins Camk2a, Camk2b, Camk2d, and Camk2g were all upregulated with many upregulated Kub sites. These proteins not only play important roles in the "calcium signaling pathway" and "long-term potentiation" but also act as kinases and scaffolding proteins in the glutamatergic synaptic cytoplasm. Camk2a contained the most upregulated ubiquitination sites among the isoforms and plays a unique role in neuronal plasticity and memory. Calcium signaling is an important component of glutamatergic synaptic signaling, and Camk2a recognizes calcium signals and translates them into the corresponding biochemical signals.[55]

In addition to the proteins mentioned previously, numerous additional proteins in these pathways exhibited proteomic and ubiquitinomic alterations as a result of SARS-CoV-2 infection. In the "glutamatergic synapse" pathway, the upregulated protein Dlg4 (contains 11 upregulated Kub sites: K264, K138, K403, K380, K299, K157, K544, K663, K558, K202, and K168) is a postsynaptic scaffolding protein that plays key roles in synaptogenesis and synaptic plasticity.[56,57] The upregulated proteins Grin2a, which contains the upregulated Kub sites K1340, K1355, K1235, K938, K1352, and K1456, and Grin2b, which contains the upregulated Kub sites K1045, K947, K1426, K1021, K1140, K1041, and K1199, are components of NMDA receptor complexes and play roles in slow excitatory postsynaptic currents, long-term synaptic potentiation, and learning.[58,59] Slc1a2, which contains the upregulated Kub site K569, facilitates the rapid clearance of glutamate released from the synaptic cleft and terminates the postsynaptic action of glutamate.[60] Pla2g4a, which contains the upregulated Kub site K371, plays an important role in membrane lipid remodeling and the production of inflammatory lipid mediators,[61] The upregulated protein Slc17a7, which contains the upregulated Kub sites K283 and K290, is a multipurpose transporter that transports L-glutamate and other ions, such as chloride, protons, potassium, sodium, and phosphate.[62–64] The upregulated protein Plcb1, which contains the upregulated Kub site K30, can mediate intracellular signaling downstream of G protein-coupled receptors.[65] The upregulated protein Ppp3ca (containing the upregulated Kub site K143) is a calcium-dependent calmodulin-stimulated protein phosphatase that has a significant impact on intracellular Ca^{2+}-mediated signal transduction.[66] Adcy6, which contains the upregulated Kub site K931, can catalyze the formation of

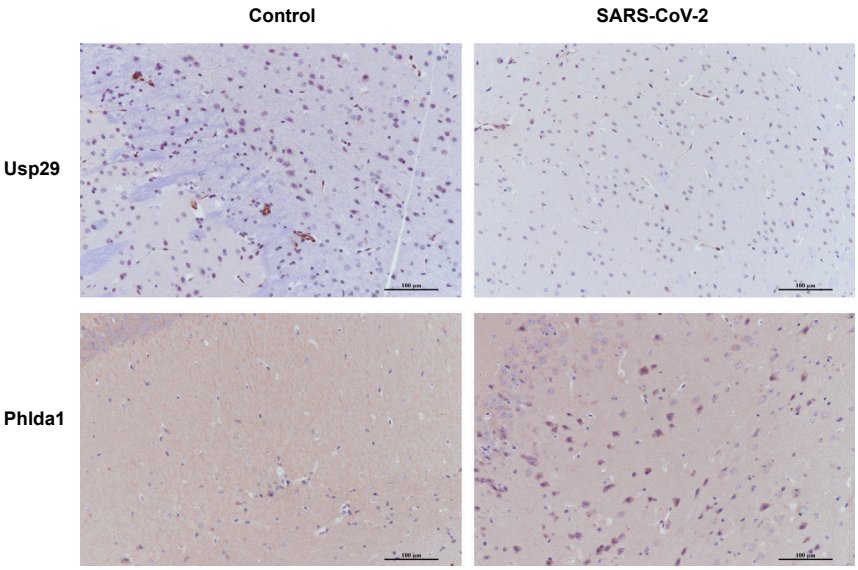

Figure 6. Representative images of Usp29 and Phlda1 immunohistochemical staining in control and SARS-CoV-2-infected mouse brain cortex tissues (scale bar, 100 μm)

cAMP, a signaling molecule downstream of G protein-coupled receptors.[67,68] Glul, which contains the upregulated Kub site K95, regulates toxic ammonia levels in the brain and converts neurotoxic glutamate to harmless glutamine.[69] Among these proteins, Grin2a, Plcb1, and Ppp3ca were also involved in the "calcium signaling" pathway, while Grin2a, Grin2b, Plcb1, and Ppp3ca were also involved in the "long-term potentiation" pathway.

E3 ubiquitin-protein ligases specifically recognize substrates and bind tightly to ubiquitin for ubiquitination. There are three main categories of E3 ubiquitin-protein ligases, which have different structures but can all transfer ubiquitin from E2 enzymes to substrates. The vast majority of E3s (approximately 600) are members of the novel gene (RING)-type family. The homologous to E6AP C-terminus (HECT)-type E3 ubiquitin-protein ligases and the RBR (RING between RING) are smaller families with 28 and 14 members, respectively.[70] TNF receptor-associated factor 2 (Traf2) is an E3 ubiquitin-protein ligase in the RING family, but it can also be ubiquitinated by the E3 ubiquitin-protein ligase Birc2 and degraded by the proteasome. In addition, during TNF stimulation, Traf2 may self-ubiquitinate and be altered by the K63 polyubiquitin chain, which is essential for the JNK signaling pathway. These K63 polyubiquitin chains may be removed by upregulated DUB Cyld.[71] The nuclear factor kappa B (NF-κB) signaling pathway has a significant impact on the regulation of innate immunity, acquired immunity, the inflammatory response, and tumorigenesis and can be divided into the canonical NF-κB signaling pathway and the noncanonical NF-κB signaling pathway.[72] Traf2 is a key regulatory factor of both the canonical and noncanonical NF-κB signaling pathways.[71] However, its significant upregulation in the cerebral cortex of K18-hACE2 mice after SARS-CoV-2 infection alone cannot explain the downregulation of the nuclear factor NF-κB p65 subunit Rela. The decrease in Rela levels may be related to the downregulation of TNF receptor-associated factor 3 (Traf3), the TNF receptor type 1-associated DEATH domain protein Tradd and the deubiquitinating enzyme Cyld and the upregulation of TNF alpha-induced protein 3 (Tnfaip3).[71,73] In addition, the upregulated E3 ubiquitin-protein ligase Hace1 is a tumor suppressor in different cancers[74] and the mutation of the E3 ubiquitin-protein ligase Hecw2 (an upregulated protein) is linked to epilepsy, developmental deterioration, and intellectual disability.[75] Moreover, the downregulated nitric oxide synthase-interacting protein (E3 ubiquitin-protein ligase NOSIP) also contributes to neuronal development, craniofacial development, mitosis, apoptosis, and cell proliferation in the nervous system, and is associated with diseases such as osteoporosis and arteriosclerosis. NOSIP can regulate the activity of the protein phosphatase 2A catalytic subunit PP2Ac (serine/threonine-protein phosphatase 2A catalytic subunit alpha isoform Ppp2ca, which contains the downregulated Kub site K21) by mediating ubiquitination.[76–80] Furthermore, we used UbiBrowser 2.0 to determine the reported interactions between E3 ubiquitin-protein ligases, DUBs, and substrate proteins. These substrate proteins were proteins with differentially expressed Kub sites (Figure S5 and Table S16). Tnfaip3 was the only enzyme that exhibited changes in expression. Moreover, several other E3 ubiquitin-protein ligases work together to regulate mitogen-activated protein kinase kinase kinase 5 (Map3k5) ubiquitination. Map3k5 is crucial for the appropriate functioning of the innate immune response, which is necessary for the host's protection against a variety of pathogens. Map3k5 mediates signaling from various stressors (e.g., oxidative stress) and inflammatory signals mediated by receptors, such as tumor necrosis factor (TNF) or lipopolysaccharide (LPS).[81,82]

In conclusion, this study provides comprehensive proteome and ubiquitinome data on the brain cortex in the K18-*hACE2* mouse model after SARS-CoV-2 infection. In this study, 5,220 quantifiable Kub sites were identified in 2,023 proteins. The results demonstrated that SARS-CoV-2 infection may harm the nervous system by regulating the expression of important proteins or ubiquitination in pathways such as the "glutamatergic synapse" pathway. Viral proteins may interact with several proteins and Kub sites in the brain cortexes of

K18-*hACE2* mice. Moreover, we found several E3 ubiquitin-protein ligases/DUBs that may act on the nervous system in the brain by altering ubiquitination. This study provides the first demonstration of ubiquitination in SARS-CoV-2-infected brain cortexes of K18-*hACE2* model mice and thus lays the groundwork for exploring the pathogenic processes of and treatment options for neurological consequences after COVID-19.

Limitations of the study

We note that our study has several limitations. Due to the shortage of COVID-19 patient tissues, we used brain cortexes from transgenic K18-*hACE2* mice, but the ubiquitinomes of mice infected with SARS-CoV-2 are somewhat different from those of humans, which reduces the reliability of our results. In addition, it has been shown that viral proteins can be ubiquitinated in lung epithelial cells after SARS-CoV-2 infection; however, in the brain cortex, no Kub viral proteins were found, and only a few nonubiquitinated proteins were identified (the ORF1ab polyprotein, surface glycoprotein, membrane glycoprotein, ORF3a protein, ORF8 protein, truncated ORF7a protein, and N protein).

STAR★METHODS

Detailed methods are provided in the online version of this paper and include the following:

- KEY RESOURCES TABLE
- RESOURCE AVAILABILITY
  - Lead contact
  - Materials availability
  - Data and code availability
- EXPERIMENTAL MODEL AND STUDY PARTICIPANT DETAILS
  - Ethics statement
  - Virus amplification and identification
  - Mouse experiments
- METHOD DETAILS
  - Extraction and quantification of viral RNA
  - Protein extraction
  - Trypsin digestion
  - HPLC classification
  - Affinity enrichment
  - LC-MS/MS analysis
  - Database search
  - Bioinformatics analysis
  - Immunohistochemical staining
- QUANTIFICATION AND STATISTICAL ANALYSIS

SUPPLEMENTAL INFORMATION

Supplemental information can be found online at https://doi.org/10.1016/j.isci.2024.110602.

ACKNOWLEDGMENTS

This study was supported by grants from the Chinese Academy of Medical Sciences Innovation Fund for Medical Sciences (CIFMS2022-I2M-JB-003).

AUTHOR CONTRIBUTIONS

Q.W. and W.P.hare the first authorship. J.Y. and J.L.: conceptualization, resources, formal analysis, writing – review & editing, supervision, and project administration. J.L. and W.P.: methodology and formal analysis. Q.W.: methodology, software, formal analysis, visualization, and writing – original draft. Y.Y., Y.W., R.H., T.D., and X.Z.: formal analysis. All authors read and approved the final manuscript.

DECLARATION OF INTERESTS

The authors declare no competing interests.

Received: February 6, 2024
Revised: May 3, 2024
Accepted: July 25, 2024
Published: July 27, 2024

REFERENCES

1. Zhu, N., Zhang, D., Wang, W., Li, X., Yang, B., Song, J., Zhao, X., Huang, B., Shi, W., Lu, R., et al. (2020). A Novel Coronavirus from Patients with Pneumonia in China, 2019. N. Engl. J. Med. *382*, 727–733. https://doi.org/10.1056/NEJMoa2001017.
2. Stukalov, A., Girault, V., Grass, V., Karayel, O., Bergant, V., Urban, C., Haas, D.A., Huang, Y., Oubraham, L., Wang, A., et al. (2021). Multilevel proteomics reveals host perturbations by SARS-CoV-2 and SARS-CoV. Nature *594*, 246–252. https://doi.org/10.1038/s41586-021-03493-4.
3. Dai, X., Cao, X., Jiang, Q., Wu, B., Lou, T., Shao, Y., Hu, Y., and Lan, Q. (2023). Neurological complications of COVID-19. QJM *116*, 161–180. https://doi.org/10.1093/qjmed/hcac272.
4. Hershko, A., and Ciechanover, A. (1998). The ubiquitin system. Annu. Rev. Biochem. *67*, 425–479. https://doi.org/10.1146/annurev.biochem.67.1.425.
5. Dang, F., Nie, L., and Wei, W. (2021). Ubiquitin signaling in cell cycle control and tumorigenesis. Cell Death Differ. *28*, 427–438. https://doi.org/10.1038/s41418-020-00648-0.
6. Wilkinson, K.D. (2000). Ubiquitination and deubiquitination: Targeting of proteins for degradation by the proteasome. Semin. Cell Dev. Biol. *11*, 141–148. https://doi.org/10.1006/scdb.2000.0164.
7. Hoeller, D., and Dikic, I. (2009). Targeting the ubiquitin system in cancer therapy. Nature *458*, 438–444. https://doi.org/10.1038/nature07960.
8. Udeshi, N.D., Mani, D.C., Satpathy, S., Fereshetian, S., Gasser, J.A., Svinkina, T., Olive, M.E., Ebert, B.L., Mertins, P., and Carr, S.A. (2020). Rapid and deep-scale ubiquitylation profiling for biology and translational research. Nat. Commun. *11*, 359. https://doi.org/10.1038/s41467-019-14175-1.
9. He, F., Zhang, L., Qi, G., Zhang, Q., Cai, H., Li, T., Li, M., Ming, J., Tian, B., and Zhang, P. (2020). Global ubiquitome analysis of substantia nigra in doubly-mutant human alpha-synuclein transgenic mice. Behav. Brain Res. *380*, 112436. https://doi.org/10.1016/j.bbr.2019.112436.
10. Key, J., Mueller, A.K., Gispert, S., Matschke, L., Wittig, I., Corti, O., Münch, C., Decher, N., and Auburger, G. (2019). Ubiquitylome profiling of Parkin-null brain reveals dysregulation of calcium homeostasis factors ATP1A2, Hippocalcin and GNA11, reflected by altered firing of noradrenergic neurons. Neurobiol. Dis. *127*, 114–130. https://doi.org/10.1016/j.nbd.2019.02.008.
11. Menon, S., Goldfarb, D., Cousins, E.M., Major, M.B., and Gupton, S.L. (2020). The ubiquitylome of developing cortical neurons. MicroPubl. Biol. *2020*. https://doi.org/10.17912/micropub.biology.000333.
12. Rose, C.M., Isasa, M., Ordureau, A., Prado, M.A., Beausoleil, S.A., Jedrychowski, M.P., Finley, D.J., Harper, J.W., and Gygi, S.P. (2016). Highly Multiplexed Quantitative Mass Spectrometry Analysis of Ubiquitylomes. Cell Syst. *3*, 395–403.e4. https://doi.org/10.1016/j.cels.2016.08.009.
13. Sap, K.A., Guler, A.T., Bezstarosti, K., Bury, A.E., Juenemann, K., Demmers, J.A., and Reits, E.A. (2019). Global Proteome and Ubiquitinome Changes in the Soluble and Insoluble Fractions of Q175 Huntington Mice Brains. Mol. Cell. Proteomics *18*, 1705–1720. https://doi.org/10.1074/mcp.RA119.001486.
14. Wagner, S.A., Beli, P., Weinert, B.T., Schölz, C., Kelstrup, C.D., Young, C., Nielsen, M.L., Olsen, J.V., Brakebusch, C., and Choudhary, C. (2012). Proteomic analyses reveal divergent ubiquitylation site patterns in murine tissues. Mol. Cell. Proteomics *11*, 1578–1585. https://doi.org/10.1074/mcp.M112.017905.
15. van der Wal, L., Bezstarosti, K., Sap, K.A., Dekkers, D.H.W., Rijkers, E., Mientjes, E., Elgersma, Y., and Demmers, J.A.A. (2018). Improvement of ubiquitylation site detection by Orbitrap mass spectrometry. J. Proteomics *172*, 49–56. https://doi.org/10.1016/j.jprot.2017.10.014.
16. Jiang, M., Hua, Z., Dong, Y., Liu, Z., Thiele, C.J., and Li, Z. (2018). Quantitative ubiquitylome analysis and crosstalk with proteome/acetylome analysis identified novel pathways and targets of perifosine treatment in neuroblastoma. Transl. Cancer Res. *7*, 1548–1560. https://doi.org/10.21037/tcr.2018.11.30.
17. Abreha, M.H., Dammer, E.B., Ping, L., Zhang, T., Duong, D.M., Gearing, M., Lah, J.J., Levey, A.I., and Seyfried, N.T. (2018). Quantitative Analysis of the Brain Ubiquitylome in Alzheimer's Disease. Proteomics *18*, e1800108. https://doi.org/10.1002/pmic.201800108.
18. Zheng, J., Wong, L.Y.R., Li, K., Verma, A.K., Ortiz, M.E., Wohlford-Lenane, C., Leidinger, M.R., Knudson, C.M., Meyerholz, D.K., McCray, P.B., Jr., and Perlman, S. (2021). COVID-19 treatments and pathogenesis including anosmia in K18-hACE2 mice. Nature *589*, 603–607. https://doi.org/10.1038/s41586-020-2943-z.
19. Golden, J.W., Cline, C.R., Zeng, X., Garrison, A.R., Carey, B.D., Mucker, E.M., White, L.E., Shamblin, J.D., Brocato, R.L., Liu, J., et al. (2020). Human angiotensin-converting enzyme 2 transgenic mice infected with SARS-CoV-2 develop severe and fatal respiratory disease. JCI Insight *5*, e142032. https://doi.org/10.1172/jci.insight.142032.
20. Oladunni, F.S., Park, J.G., Pino, P.A., Gonzalez, O., Akhter, A., Allué-Guardia, A., Olmo-Fontánez, A., Gautam, S., Garcia-Vilanova, A., Ye, C., et al. (2020). Lethality of SARS-CoV-2 infection in K18 human angiotensin-converting enzyme 2 transgenic mice. Nat. Commun. *11*, 6122. https://doi.org/10.1038/s41467-020-19891-7.
21. Lopes, D.M., Llewellyn, S.K., and Harrison, I.F. (2022). Propagation of tau and alpha-synuclein in the brain: therapeutic potential of the glymphatic system. Transl. Neurodegener. *11*, 19. https://doi.org/10.1186/s40035-022-00293-2.
22. Zhang, H., Zheng, H., Zhu, J., Dong, Q., Wang, J., Fan, H., Chen, Y., Zhang, X., Han, X., Li, Q., et al. (2021). Ubiquitin-Modified Proteome of SARS-CoV-2-Infected Host Cells Reveals Insights into Virus-Host Interaction and Pathogenesis. J. Proteome Res. *20*, 2224–2239. https://doi.org/10.1021/acs.jproteome.0c00758.
23. Xu, G., Wu, Y., Xiao, T., Qi, F., Fan, L., Zhang, S., Zhou, J., He, Y., Gao, X., Zeng, H., et al. (2022). Multiomics approach reveals the ubiquitination-specific processes hijacked by SARS-CoV-2. Signal Transduct. Target. Ther. *7*, 312. https://doi.org/10.1038/s41392-022-01156-y.
24. Butler, A., Tsunoda, S., McCobb, D.P., Wei, A., and Salkoff, L. (1993). mSlo, a complex mouse gene encoding "maxi" calcium-activated potassium channels. Science *261*, 221–224. https://doi.org/10.1126/science.7687074.
25. Li, G., Mongillo, M., Chin, K.T., Harding, H., Ron, D., Marks, A.R., and Tabas, I. (2009). Role of ERO1-alpha-mediated stimulation of inositol 1,4,5-triphosphate receptor activity in endoplasmic reticulum stress-induced apoptosis. J. Cell Biol. *186*, 783–792. https://doi.org/10.1083/jcb.200904060.
26. Lindsey, A.E., Schneider, K., Simmons, D.M., Baron, R., Lee, B.S., and Kopito, R.R. (1990). Functional expression and subcellular localization of an anion exchanger cloned from choroid plexus. Proc. Natl. Acad. Sci. USA *87*, 5278–5282. https://doi.org/10.1073/pnas.87.14.5278.
27. Yasuda, T., Shibasaki, T., Minami, K., Takahashi, H., Mizoguchi, A., Uriu, Y., Numata, T., Mori, Y., Miyazaki, J.I., Miki, T., and Seino, S. (2010). Rim2alpha determines docking and priming states in insulin granule exocytosis. Cell Metab. *12*, 117–129. https://doi.org/10.1016/j.cmet.2010.05.017.
28. Martin, L.B., Shewan, A., Millar, C.A., Gould, G.W., and James, D.E. (1998). Vesicle-associated membrane protein 2 plays a specific role in the insulin-dependent trafficking of the facilitative glucose transporter GLUT4 in 3T3-L1 adipocytes. J. Biol. Chem. *273*, 1444–1452. https://doi.org/10.1074/jbc.273.3.1444.
29. Guo, F., He, H., Fu, Z.C., Huang, S., Chen, T., Papasian, C.J., Morse, L.R., Xu, Y., Battaglino, R.A., Yang, X.F., et al. (2015). Adipocyte-derived PAMM suppresses macrophage inflammation by inhibiting MAPK signalling. Biochem. J. *472*, 309–318. https://doi.org/10.1042/BJ20150019.
30. Mochly-Rosen, D., Das, K., and Grimes, K.V. (2012). Protein kinase C, an elusive therapeutic target? Nat. Rev. Drug Discov. *11*, 937–957. https://doi.org/10.1038/nrd3871.
31. Janz, R., Südhof, T.C., Hammer, R.E., Unni, V., Siegelbaum, S.A., and Bolshakov, V.Y. (1999). Essential roles in synaptic plasticity for synaptogyrin I and synaptophysin I. Neuron *24*, 687–700. https://doi.org/10.1016/s0896-6273(00)81122-8.
32. Bai, C., Zhong, Q., and Gao, G.F. (2022). Overview of SARS-CoV-2 genome-encoded proteins. Sci. China Life Sci. *65*, 280–294. https://doi.org/10.1007/s11427-021-1964-4.
33. Gordon, D.E., Jang, G.M., Bouhaddou, M., Xu, J., Obernier, K., White, K.M., O'Meara, M.J., Rezelj, V.V., Guo, J.Z., Swaney, D.L., et al. (2020). A SARS-CoV-2 protein interaction map reveals targets for drug repurposing. Nature *583*, 459–468. https://doi.org/10.1038/s41586-020-2286-9.
34. Zhang, Q., Tang, Z., An, R., Ye, L., and Zhong, B. (2020). USP29 maintains the stability of cGAS and promotes cellular antiviral responses and autoimmunity. Cell Res. *30*, 914–927. https://doi.org/10.1038/s41422-020-0341-6.
35. Gao, W., Wang, L., Ju, X., Zhao, S., Li, Z., Su, M., Xu, J., Wang, P., Ding, Q., Lv, G., and Zhang, W. (2022). The Deubiquitinase USP29 Promotes SARS-CoV-2 Virulence by Preventing Proteasome Degradation of ORF9b. mBio *13*, e0130022. https://doi.org/10.1128/mbio.01300-22.

36. Shu, L., and Du, C. (2022). PHLDA1 promotes sevoflurane-induced pyroptosis of neuronal cells in developing rats through TRAF6-mediated activation of Rac1. Neurotoxicology *93*, 140–151. https://doi.org/10.1016/j.neuro.2022.09.007.
37. Ceban, F., Ling, S., Lui, L.M.W., Lee, Y., Gill, H., Teopiz, K.M., Rodrigues, N.B., Subramaniapillai, M., Di Vincenzo, J.D., Cao, B., et al. (2022). Fatigue and cognitive impairment in Post-COVID-19 Syndrome: A systematic review and meta-analysis. Brain Behav. Immun. *101*, 93–135. https://doi.org/10.1016/j.bbi.2021.12.020.
38. Conti, F., and Weinberg, R.J. (1999). Shaping excitation at glutamatergic synapses. Trends Neurosci. *22*, 451–458. https://doi.org/10.1016/S0166-2236(99)01445-9.
39. Greene, C., Connolly, R., Brennan, D., Laffan, A., O'Keeffe, E., Zaporojan, L., O'Callaghan, J., Thomson, B., Connolly, E., Argue, R., et al. (2024). Blood-brain barrier disruption and sustained systemic inflammation in individuals with long COVID-associated cognitive impairment. Nat. Neurosci. *27*, 421–432. https://doi.org/10.1038/s41593-024-01576-9.
40. Rodriguez, L., and Brodin, P. (2024). Immune system perturbations in patients with long COVID. Trends Mol. Med. *30*, 200–201. https://doi.org/10.1016/j.molmed.2023.12.008.
41. Suprewicz, Ł., Fiedoruk, K., Czarnowska, A., Sadowski, M., Strzelecka, A., Galie, P.A., Janmey, P.A., Kułakowska, A., and Bucki, R. (2023). Blood-brain barrier function in response to SARS-CoV-2 and its spike protein. Neurol. Neurochir. Pol. *57*, 14–25. https://doi.org/10.5603/PJNNS.a2023.0014.
42. Ostermann, P.N., and Schaal, H. (2023). Human brain organoids to explore SARS-CoV-2-induced effects on the central nervous system. Rev. Med. Virol. *33*, e2430. https://doi.org/10.1002/rmv.2430.
43. Schweizer, L., Schaller, T., Zwiebel, M., Karayel, Ö., Müller-Reif, J.B., Zeng, W.F., Dintner, S., Nordmann, T.M., Hirschbühl, K., Märkl, B., et al. (2023). Quantitative multiorgan proteomics of fatal COVID-19 uncovers tissue-specific effects beyond inflammation. EMBO Mol. Med. *15*, e17459. https://doi.org/10.15252/emmm.202317459.
44. Yesilkaya, U.H., Sen, M., and Balcioglu, Y.H. (2021). COVID-19-related cognitive dysfunction may be associated with transient disruption in the DLPFC glutamatergic pathway. J. Clin. Neurosci. *87*, 153–155. https://doi.org/10.1016/j.jocn.2021.03.007.
45. Chaganti, J., Poudel, G., Cysique, L.A., Dore, G.J., Kelleher, A., Matthews, G., Darley, D., Byrne, A., Jakabek, D., Zhang, X., et al. (2024). Blood brain barrier disruption and glutamatergic excitotoxicity in post-acute sequelae of SARS COV-2 infection cognitive impairment: potential biomarkers and a window into pathogenesis. Front. Neurol. *15*, 1350848.
46. Manganotti, P., Michelutti, M., Furlanis, G., Deodato, M., and Buoite Stella, A. (2023). Deficient GABABergic and glutamatergic excitability in the motor cortex of patients with long-COVID and cognitive impairment. Clin. Neurophysiol. *151*, 83–91. https://doi.org/10.1016/j.clinph.2023.04.010.
47. Partiot, E., Hirschler, A., Colomb, S., Lutz, W., Claeys, T., Delalande, F., Deffieu, M.S., Bare, Y., Roels, J.R.E., Gorda, B., et al. (2024). Brain exposure to SARS-CoV-2 virions perturbs synaptic homeostasis. Nat. Microbiol. *9*, 1189–1206. https://doi.org/10.1038/s41564-024-01657-2.
48. Spillantini, M.G., Schmidt, M.L., Lee, V.M., Trojanowski, J.Q., Jakes, R., and Goedert, M. (1997). Alpha-synuclein in Lewy bodies. Nature *388*, 839–840. https://doi.org/10.1038/42166.
49. Dickson, D.W. (2012). Parkinson's disease and parkinsonism: neuropathology. Cold Spring Harb. Perspect. Med. *2*, a009258. https://doi.org/10.1101/cshperspect.a009258.
50. Goldman, J.G., and Postuma, R. (2014). Premotor and nonmotor features of Parkinson's disease. Curr. Opin. Neurol. *27*, 434–441. https://doi.org/10.1097/WCO.0000000000000112.
51. Sveinbjornsdottir, S. (2016). The clinical symptoms of Parkinson's disease. J. Neurochem. *139*, 318–324. https://doi.org/10.1111/jnc.13691.
52. Schapira, A.H.V., Chaudhuri, K.R., and Jenner, P. (2017). Non-motor features of Parkinson disease. Nat. Rev. Neurosci. *18*, 509. https://doi.org/10.1038/nrn.2017.91.
53. Chegao, A., Guarda, M., Alexandre, B.M., Shvachiy, L., Temido-Ferreira, M., Marques-Morgado, I., Fernandes Gomes, B., Matthiesen, R., Lopes, L.V., Florindo, P.R., et al. (2022). Glycation modulates glutamatergic signaling and exacerbates Parkinson's disease-like phenotypes. NPJ Parkinsons Dis *8*, 51. https://doi.org/10.1038/s41531-022-00314-x.
54. Conway, M.E. (2020). Alzheimer's disease: targeting the glutamatergic system. Biogerontology *21*, 257–274. https://doi.org/10.1007/s10522-020-09860-4.
55. Mohanan, A.G., Gunasekaran, S., Jacob, R.S., and Omkumar, R.V. (2022). Role of Ca2+/Calmodulin-Dependent Protein Kinase Type II in Mediating Function and Dysfunction at Glutamatergic Synapses. Front. Mol. Neurosci. *15*, 855752.
56. He, J., Bellini, M., Xu, J., Castleberry, A.M., and Hall, R.A. (2004). Interaction with cystic fibrosis transmembrane conductance regulator-associated ligand (CAL) inhibits beta1-adrenergic receptor surface expression. J. Biol. Chem. *279*, 50190–50196. https://doi.org/10.1074/jbc.M404876200.
57. Migaud, M., Charlesworth, P., Dempster, M., Webster, L.C., Watabe, A.M., Makhinson, M., He, Y., Ramsay, M.F., Morris, R.G., Morrison, J.H., et al. (1998). Enhanced long-term potentiation and impaired learning in mice with mutant postsynaptic density-95 protein. Nature *396*, 433–439. https://doi.org/10.1038/24790.
58. Sakimura, K., Kutsuwada, T., Ito, I., Manabe, T., Takayama, C., Kushiya, E., Yagi, T., Aizawa, S., Inoue, Y., Sugiyama, H., et al. (1995). Reduced hippocampal LTP and spatial learning in mice lacking NMDA receptor epsilon 1 subunit. Nature *373*, 151–155. https://doi.org/10.1038/373151a0.
59. Kadotani, H., Hirano, T., Masugi, M., Nakamura, K., Nakao, K., Katsuki, M., and Nakanishi, S. (1996). Motor discoordination results from combined gene disruption of the NMDA receptor NR2A and NR2C subunits, but not from single disruption of the NR2A or NR2C subunit. J. Neurosci. *16*, 7859–7867. https://doi.org/10.1523/JNEUROSCI.16-24-07859.1996.
60. Tanaka, K., Watase, K., Manabe, T., Yamada, K., Watanabe, M., Takahashi, K., Iwama, H., Nishikawa, T., Ichihara, N., Kikuchi, T., et al. (1997). Epilepsy and exacerbation of brain injury in mice lacking the glutamate transporter GLT-1. Science *276*, 1699–1702. https://doi.org/10.1126/science.276.5319.1699.
61. Bonventre, J.V., Huang, Z., Taheri, M.R., O'Leary, E., Li, E., Moskowitz, M.A., and Sapirstein, A. (1997). Reduced fertility and postischaemic brain injury in mice deficient in cytosolic phospholipase A2. Nature *390*, 622–625. https://doi.org/10.1038/37635.
62. Preobraschenski, J., Cheret, C., Ganzella, M., Zander, J.F., Richter, K., Schenck, S., Jahn, R., and Ahnert-Hilger, G. (2018). Dual and Direction-Selective Mechanisms of Phosphate Transport by the Vesicular Glutamate Transporter. Cell Rep. *23*, 535–545. https://doi.org/10.1016/j.celrep.2018.03.055.
63. Preobraschenski, J., Zander, J.F., Suzuki, T., Ahnert-Hilger, G., and Jahn, R. (2014). Vesicular glutamate transporters use flexible anion and cation binding sites for efficient accumulation of neurotransmitter. Neuron *84*, 1287–1301. https://doi.org/10.1016/j.neuron.2014.11.008.
64. Cheret, C., Ganzella, M., Preobraschenski, J., Jahn, R., and Ahnert-Hilger, G. (2021). Vesicular Glutamate Transporters (SLCA17 A6, 7, 8) Control Synaptic Phosphate Levels. Cell Rep. *34*, 108623. https://doi.org/10.1016/j.celrep.2020.108623.
65. Beard, R.S., Jr., Yang, X., Meegan, J.E., Overstreet, J.W., Yang, C.G.Y., Elliott, J.A., Reynolds, J.J., Cha, B.J., Pivetti, C.D., Mitchell, D.A., et al. (2016). Palmitoyl acyltransferase DHHC21 mediates endothelial dysfunction in systemic inflammatory response syndrome. Nat. Commun. *7*, 12823. https://doi.org/10.1038/ncomms12823.
66. Fruman, D.A., Pai, S.Y., Burakoff, S.J., and Bierer, B.E. (1995). Characterization of a mutant calcineurin A alpha gene expressed by EL4 lymphoma cells. Mol. Cell Biol. *15*, 3857–3863. https://doi.org/10.1128/MCB.15.7.3857.
67. Tang, T., Gao, M.H., Lai, N.C., Firth, A.L., Takahashi, T., Guo, T., Yuan, J.X.J., Roth, D.M., and Hammond, H.K. (2008). Adenylyl cyclase type 6 deletion decreases left ventricular function via impaired calcium handling. Circulation *117*, 61–69. https://doi.org/10.1161/CIRCULATIONAHA.107.730069.
68. Bogard, A.S., Birg, A.V., and Ostrom, R.S. (2014). Non-raft adenylyl cyclase 2 defines a cAMP signaling compartment that selectively regulates IL-6 expression in airway smooth muscle cells: differential regulation of gene expression by AC isoforms. N-S Arch Pharmacol *387*, 329–339. https://doi.org/10.1007/s00210-013-0950-4.
69. Qvartskhava, N., Lang, P.A., Görg, B., Pozdeev, V.I., Ortiz, M.P., Lang, K.S., Bidmon, H.J., Lang, E., Leibrock, C.B., Herebian, D., et al. (2015). Hyperammonemia in gene-targeted mice lacking functional hepatic glutamine synthetase. Proc. Natl. Acad. Sci. USA *112*, 5521–5526. https://doi.org/10.1073/pnas.1423968112.
70. Berndsen, C.E., and Wolberger, C. (2014). New insights into ubiquitin E3 ligase mechanism. Nat. Struct. Mol. Biol. *21*, 301–307. https://doi.org/10.1038/nsmb.2780.
71. Borghi, A., Verstrepen, L., and Beyaert, R. (2016). TRAF2 multitasking in TNF receptor-induced signaling to NF-kappaB, MAP kinases and cell death. Biochem. Pharmacol. *116*, 1–10. https://doi.org/10.1016/j.bcp.2016.03.009.

72. Basseres, D.S., and Baldwin, A.S. (2006). Nuclear factor-kappaB and inhibitor of kappaB kinase pathways in oncogenic initiation and progression. Oncogene *25*, 6817–6830. https://doi.org/10.1038/sj.onc.1209942.
73. Lork, M., Verhelst, K., and Beyaert, R. (2017). CYLD, A20 and OTULIN deubiquitinases in NF-kappaB signaling and cell death: so similar, yet so different. Cell Death Differ. *24*, 1172–1183. https://doi.org/10.1038/cdd.2017.46.
74. Da, C., Pu, J., Liu, Z., Wei, J., Qu, Y., Wu, Y., Shi, B., Yang, J., He, N., and Hou, P. (2021). HACE1-mediated NRF2 activation causes enhanced malignant phenotypes and decreased radiosensitivity of glioma cells. Signal Transduct. Target. Ther. *6*, 399. https://doi.org/10.1038/s41392-021-00793-z.
75. Ullman, N.L., Smith-Hicks, C.L., Desai, S., and Stafstrom, C.E. (2018). De Novo HECW2 Mutation Associated With Epilepsy, Developmental Decline, and Intellectual Disability: Case Report and Review of Literature. Pediatr. Neurol. *85*, 76–78. https://doi.org/10.1016/j.pediatrneurol.2018.03.005.
76. Hoffmeister, M., Krieg, J., Ehrke, A., Seigfried, F.A., Wischmann, L., Dietmann, P., Kühl, S.J., and Oess, S. (2017). Developmental neurogenesis in mouse and Xenopus is impaired in the absence of Nosip. Dev. Biol. *429*, 200–212. https://doi.org/10.1016/j.ydbio.2017.06.026.
77. Porschke, M., Rodriguez-Gonzalez, I., Parfentev, I., Urlaub, H., and Kehlenbach, R.H. (2023). Transportin 1 is a major nuclear import receptor of the nitric oxide synthase interacting protein. J. Biol. Chem. *299*, 102932. https://doi.org/10.1016/j.jbc.2023.102932.
78. Mishra, B.H., Mishra, P.P., Raitoharju, E., Marttila, S., Mononen, N., Sievänen, H., Viikari, J., Juonala, M., Laaksonen, M., Hutri-Kähönen, N., et al. (2021). Modular genome-wide gene expression architecture shared by early traits of osteoporosis and atherosclerosis in the Young Finns Study. Sci. Rep. *11*, 7111. https://doi.org/10.1038/s41598-021-86536-0.
79. Hoffmeister, M., Prelle, C., Küchler, P., Kovacevic, I., Moser, M., Müller-Esterl, W., and Oess, S. (2014). The ubiquitin E3 ligase NOSIP modulates protein phosphatase 2A activity in craniofacial development. PLoS One *9*, e116150. https://doi.org/10.1371/journal.pone.0116150.
80. Schleicher, M., Brundin, F., Gross, S., Müller-Esterl, W., and Oess, S. (2005). Cell cycle-regulated inactivation of endothelial NO synthase through NOSIP-dependent targeting to the cytoskeleton. Mol. Cell Biol. *25*, 8251–8258. https://doi.org/10.1128/MCB.25.18.8251-8258.2005.
81. Takeda, K., Matsuzawa, A., Nishitoh, H., Tobiume, K., Kishida, S., Ninomiya-Tsuji, J., Matsumoto, K., and Ichijo, H. (2004). Involvement of ASK1 in Ca2+-induced p38 MAP kinase activation. EMBO Rep. *5*, 161–166. https://doi.org/10.1038/sj.embor.7400072.
82. Matsuzawa, A., Saegusa, K., Noguchi, T., Sadamitsu, C., Nishitoh, H., Nagai, S., Koyasu, S., Matsumoto, K., Takeda, K., and Ichijo, H. (2005). ROS-dependent activation of the TRAF6-ASK1-p38 pathway is selectively required for TLR4-mediated innate immunity. Nat. Immunol. *6*, 587–592. https://doi.org/10.1038/ni1200.
83. Ma, J., Chen, T., Wu, S., Yang, C., Bai, M., Shu, K., Li, K., Zhang, G., Jin, Z., He, F., et al. (2019). iProX: an integrated proteome resource. Nucleic Acids Res. *47*, D1211–D1217. https://doi.org/10.1093/nar/gky869.
84. Bao, L., Deng, W., Huang, B., Gao, H., Liu, J., Ren, L., Wei, Q., Yu, P., Xu, Y., Qi, F., et al. (2020). The pathogenicity of SARS-CoV-2 in hACE2 transgenic mice. Nature *583*, 830–833. https://doi.org/10.1038/s41586-020-2312-y.
85. Liu, J.F., Zhou, Y.N., Lu, S.Y., Yang, Y.H., Wu, S.F., Liu, D.P., Peng, X.Z., and Yang, J.T. (2022). Proteomic and phosphoproteomic profiling of COVID-19-associated lung and liver injury: a report based on rhesus macaques. Signal Transduct. Target. Ther. *7*, 27. https://doi.org/10.1038/s41392-022-00882-7.
86. Liu, J.F., Peng, W.J., Wu, Y., Yang, Y.H., Wu, S.F., Liu, D.P., Liu, J.N., and Yang, J.T. (2023). Proteomic and phosphoproteomic characteristics of the cortex, hippocampus, thalamus, lung, and kidney in COVID-19-infected female K18-hACE2 mice. EBioMedicine *90*, 104518. https://doi.org/10.1016/j.ebiom.2023.104518.
87. Du, Y., Cai, T., Li, T., Xue, P., Zhou, B., He, X., Wei, P., Liu, P., Yang, F., and Wei, T. (2015). Lysine malonylation is elevated in type 2 diabetic mouse models and enriched in metabolic associated proteins. Mol. Cell. Proteomics *14*, 227–236. https://doi.org/10.1074/mcp.M114.041947.
88. Tyanova, S., Temu, T., and Cox, J. (2016). The MaxQuant computational platform for mass spectrometry-based shotgun proteomics. Nat. Protoc. *11*, 2301–2319. https://doi.org/10.1038/nprot.2016.136.
89. Liu, J.F., Wu, S.F., Liu, S., Sun, X., Wang, X.M., Xu, P., Chen, H.Z., and Yang, J.T. (2020). Global Lysine Crotonylation Profiling of Mouse Liver. Proteomics *20*, e2000049. https://doi.org/10.1002/pmic.202000049.
90. Cheng, A., Grant, C.E., Noble, W.S., and Bailey, T.L. (2019). MoMo: discovery of statistically significant post-translational modification motifs. Bioinformatics *35*, 2774–2782. https://doi.org/10.1093/bioinformatics/bty1058.
91. Wu, T., Hu, E., Xu, S., Chen, M., Guo, P., Dai, Z., Feng, T., Zhou, L., Tang, W., Zhan, L., et al. (2021). clusterProfiler 4.0: A universal enrichment tool for interpreting omics data. Innovation *2*, 100141. https://doi.org/10.1016/j.xinn.2021.100141.
92. Wang, X., Li, Y., He, M., Kong, X., Jiang, P., Liu, X., Diao, L., Zhang, X., Li, H., Ling, X., et al. (2022). UbiBrowser 2.0: a comprehensive resource for proteome-wide known and predicted ubiquitin ligase/deubiquitinase-substrate interactions in eukaryotic species. Nucleic Acids Res. *50*, D719–D728. https://doi.org/10.1093/nar/gkab962.
93. Li, Y., Xie, P., Lu, L., Wang, J., Diao, L., Liu, Z., Guo, F., He, Y., Liu, Y., Huang, Q., et al. (2017). An integrated bioinformatics platform for investigating the human E3 ubiquitin ligase-substrate interaction network. Nat. Commun. *8*, 347. https://doi.org/10.1038/s41467-017-00299-9.
94. Wang, S., Zhong, Y., Cheng, J., and Yang, H. (2021). EnrichVisBox: A Versatile and Powerful Web Toolbox for Visualizing Complex Functional Enrichment Results of Omics Data. J. Comput. Biol. *28*, 922–930. https://doi.org/10.1089/cmb.2020.0564.

STAR★METHODS

KEY RESOURCES TABLE

REAGENT or RESOURCE	SOURCE	IDENTIFIER
Antibodies		
Ubiquitinated resin	Hangzhou Jingjie Biotechnology PTM BIO.	Cat#PTM-1104
Anti-USP29 polyclonal antibody	Invitrogen	PA5-104441
Anti-PHLDA1 polyclonal antibody	Invitrogen	PA5-119776
HRP-labeled goat anti-rabbit IgG secondary antibody	Beijing ZSGB Biotechnology	PV9001
Bacterial and virus strains		
SARS-CoV-2 strain HB-01	from W. Tan	GISAID identifier: BetaCoV/Wuhan/IVDC-HB-01/2020|EPI_ISL_402119); the China National Microbiological Data Center accession number NMDC10013001; genome accession number:MDC60013002-01
Chemicals, peptides, and recombinant proteins		
Dulbecco's modified Eagle's medium (DMEM)	Invitrogen	Cat#11965092
Fetal bovine serum (FBS)	Deoxycholate	Cat#F8318
Penicillin and Streptomycin	Sigma–Aldrich	Cat#V900929
Avertin	Sigma–Aldrich	Cat#T48402
PBS	Solarbio	Cat#P1020
Tris•HCl	Sigma–Aldrich	Cat#RES3098T-B701X
Sodium chlorid	Sigma–Aldrich	Cat#S9888-500G
Sodium dodecyl sulfate, SDS	Solarbio	Cat#S8010-500g
Trichostatin A, TSA	MedChemExpress	Cat#HY-15144
Nicotinamide, NAM	Sigma-Aldrich	Cat#N0636-500g
Triton X-100	Sigma-Aldrich	Cat#X100PC
Deoxycholate	Sigma-Aldrich	Cat#D6750
Acetone	Hangzhou Hannuo Chemical	N/A
Triethylammonium bicarbonate buffer, TEAB	Sigma-Aldrich	Cat#T7408-500mL
Trypsin	Promega	Cat#V5117
DL-Dithiothreitol, DTT	Sigma–Aldrich	Cat#D9163-25G
Iodoacetamide, IAM	Sigma–Aldrich	Cat#V900335-5G
EDTA	Sigma–Aldrich	Cat# E6758
NP-40	Sigma–Aldrich	Cat# I3021
Trifluoroacetic acid, TFA	Sigma-Aldrich	Cat#302031-1L
Acetonitrile	Thermo Fisher Scientific	Cat#204433
Formic acid	Sigma-Aldrich	Cat# 56302
Critical commercial assays		
RNeasy mini kit	Qiagen	Cat# 74104
PrimerScript RT Reagent Kit	TaKaRa	Cat# RR037A
PowerUp SYBR Green Master Mix Kit	Applied Biosystems	Cat#A25742
BCA kit	Beyotime Biotechnology	Cat#P0011

(*Continued on next page*)

Continued

REAGENT or RESOURCE	SOURCE	IDENTIFIER
Deposited data		
Proteome and ubiquitinome mass spectrometry data	This paper	ProteomeXchange ID: PXD042461 https://www.iprox.cn/page/PSV023.html;?url=16850750448719diL
Experimental models: Cell lines		
Vero cells	Cell Bank of Type Culture Collection of Chinese Academy of Sciences	N/A
Experimental models: Organisms/strains		
K18-*hACE2* mice	Peking Union Medical College's Institute of Laboratory Animal Science	N/A
Oligonucleotides		
Primer sequences: forward: 5′-TCGTTTCGGAAGAGAGAGT-3′, reverse: 5′-GCGCAGTAAGGAGGCTAGT-3′	This paper	N/A
Software and algorithms		
MaxQuant	www.maxquant.org/	v.2.0.3.1
MoMo	https://meme-suite.org/meme/tools/momo	v.5.5.0
R*64	https://cran.r-project.org/	v.4.3.1
R package ClusterProfiler	https://cran.r-project.org/	v. 4.8.3
STRING database	https://string-db.org/	v.11.5
Cytoscape	https://cytoscape.org/download.html	v. 3.9.1
UbiBrowser	http://ubibrowser.bio-it.cn/ubibrowser_v3/home/index	v.2.0
BLAST	https://www.ncbi.nlm.nih.gov/	v. 2.13.0
'Wu Kong' platform	https://www.omicsolution.com/wkomics/main/	v.38
BioLadder platform	https://www.bioladder.cn/web/#/pro/index	N/A

RESOURCE AVAILABILITY

Lead contact

Further information and requests for resources and reagents should be directed to and will be fulfilled by the lead contact, Juntao Yang (yangjt@pumc.edu.cn).

Materials availability

This study did not generate new unique reagents.

Data and code availability

- Data: Mass Spectrometry data have been deposited at ProteomeXchange[83] and are publicly available as of the date of publication. Accession numbers are listed in the key resources table.
- Code: This paper does not report original code.
- Additional information: Any additional information required to reanalyze the data reported in this paper is available from the lead contact upon request.

EXPERIMENTAL MODEL AND STUDY PARTICIPANT DETAILS

Ethics statement

The Institutional Animal Care and Use Committee of the Institute of Laboratory Animal Science (IACUC), Peking Union Medical College, approved all the animal procedures used in this research (IACUC number: LJN22005). All the experiments on the animals were performed at an ABSL-3 facility using HEPA-filtered isolators at the Institute of Laboratory Animal Science, Peking Union Medical College, in accordance with the National Care and Use of Animals Guidelines, which were established by the National Animal Research Authority.

Virus amplification and identification

In this study, the SARS-CoV-2 strain HB-01 was obtained from W. Tan.[1] HB-01 was extracted from Vero cells grown in DMEM (Invitrogen) supplemented with 10% FBS, 100 μg/mL streptomycin, and 100 IU/mL penicillin at 37°C and 5% CO2; subsequently, the cells were purified and stored.[84] Real-time quantitative PCR (RT−qPCR), sequencing, transmission electronic microscopy, and plaque assays were used to identify the SARS-CoV-2 strain HB-01.[85]

Mouse experiments

In this work, six female specific-pathogen-free (SPF) K18-hACE2 mice aged between six and ten months were randomly assigned to one of two groups: the SARS-CoV-2 infection group (n = 3) or the control group (n = 3). The mice were acquired from Peking Union Medical College's Institute of Laboratory Animal Science. Following abdominal anesthesia with 0.02 mL/g body weight and 2.5% avertin, mice in the SARS-CoV-2 infection group were infected with SARS-CoV-2 at 1 mL of 5.5 × 105 PFU (500 μL/nostril), while equivalent amounts of phosphate-buffered saline were injected into the mice in the control group (PBS).[85] The weight, clinical symptoms, reaction to surface stimulation, and mortality rate of the infected mice were continually monitored. At 5 dpi, the mice were dissected to cut the cerebral cortex for assessment of viral replication and pathological alterations and proteomic and ubiquitinated proteomic profiling.[84] Brain cortex tissue samples were taken and stored at −80°C.

Because ACE2 is found on the X chromosome in wild-type mice, human ACE2 was implanted on the X chromosome in K18-*hACE2* animals. Male K18-*hACE2* mice were mated with female wild-type mice to produce K18-*hACE2* mice. We only infected female K18-*hACE2* mice because human ACE2 is located only on the X chromosome in female mice.[86]

METHOD DETAILS

Extraction and quantification of viral RNA

To summarize, we produced tissue homogenates and utilized an RNeasy Mini Kit (Qiagen) to extract total RNA. We used a PrimerScript RT Reagent Kit (TaKaRa) and PowerUp SYBR Green Master Mix Kit (Applied Biosystems) to perform RT−qPCR according to the following cycle protocol: 50°C for 2 min, 95°C for 2 min, and 40 cycles of 95°C for 15 s and 60°C for 30 s, after which the temperature was 95°C for 15 s, 60°C for 1 min, and 95°C for 45 s. The primer sequences for the envelope (E) gene of SARS-CoV-2 were as follows: forward primer, 5′-TCGTTTCGGAAGAGACAGGT-3′; reverse primer, 5′-GCGCAGTAAGGATGGCTAGT-3′.[84]

Protein extraction

The brain cortex was removed from the −80°C freezer and defrosted on ice before being homogenized with beads and ultrasonically lysed. After centrifuging for 10 min at 4°C and 12000 × g, the pieces were removed, and the supernatant was transferred to a fresh centrifuge tube. A BCA kit was used to calculate the protein concentration (Beyotime Biotechnology).

Trypsin digestion

The proteins were enzymatically hydrolyzed in equal amounts (2.8 mg), and the volume was adjusted to match that of the buffer solution (50 mM Tris • HCl, 150 mM sodium chloride [Sigma−Aldrich], 1% polyethylene glycol octyl phenol ether, 1% deoxycholate, 0.1% lauryl sodium sulfate, 3 μM TSA, 50 mM NAM). An equivalent volume of precooled acetone (Hangzhou Hannuo Chemical) was added, after which the mixture was vortexed. After adding four times the volume of precooled acetone, the sample was precipitated at −20°C for 2 h. We discarded the supernatant and washed the precipitate twice with cold acetone after centrifuging it at 4500 × g for 5 min. After drying, we added 200 mM TEAB (Sigma−Aldrich) and utilized ultrasonication to dissolve the precipitate. Then, we added trypsin (Promega) at a 1:50 (protease:protein, m/m) ratio and subjected the mixture to enzymolysis for 16 h. Finally, we added 5 mM DTT (Sigma−Aldrich) to decrease the pH at 56°C for 30 min before the mixture was incubated for 15 min in darkness at ambient temperature.

HPLC classification

The proteomic samples were fractionated into 36 fractions and 10 groups, while the ubiquitinomic samples were not fractionated. The proteomic samples were separated using an Agilent 300 Extend C18 column (4.6 mm × 250 mm size, 5 μm particle size) at 214 nm with a column temperature of 35°C, 95% buffer A (2% ACN, pH 9.0 adjusted by ammonia), and 5% buffer B (98% ACN, pH 9.0 adjusted by ammonia). The column was equilibrated for 30 min, and after baseline leveling, the mixture was subjected to the graded gradient method. The peptide sample was dissolved by vortexing with 1 mL of buffer A. After centrifugation at 12000 × g for 5 min, the supernatant was centrifuged again, and the supernatant was collected for HPLC. HPLC was started to separate the sample, and the automatic collector started to collect the sample at 1 min/tube. The effective gradient of liquid-phase classification was set at 10–45 min such that tubes 11 to 46 were collected. No peptide sample fraction was taken from the remaining collection tubes after internal testing. A total of 36 tubes were collected and combined into 10 fractions (fraction 1: 11, 21, 31 and 41 min; fraction 2: 12, 22, 32 and 42 min; fraction 3: 13, 23, 33 and 43 min; fraction 4: 14, 24 and 34 min; fraction 5: 15, 25 and 35 min; fraction 6: 16, 26 and 36 min; fraction 7: 17, 27 and 37 min; fraction 8: 18, 28, 38 and 44 min; fraction 9: 19, 29, 39 and 45 min; and fraction 10: 20, 30, 40 and 46 min) and vacuum-dried.

Affinity enrichment

Affinity enrichment was required only for the ubiquitinomics analysis and not for the proteomics analysis. We dissolved the peptides in IP buffer solution (100 mM NaCl, 0.5% NP-40, 50 mM Tris-HCl, 1 mM EDTA; Sigma–Aldrich, pH 8.0), transferred the supernatant to cleaned ubiquitinated resin (PTM-1104; Jingjie Biotechnology Corporation), placed the mixture on a rotating oscillator at 4°C, and incubated the resin with rotation overnight. The resin was then washed twice with deionized water (Fisher Chemical) and four times with IP buffer solution before the peptides that were attached to the resin were eluted using 0.1% TFA (Sigma–Aldrich) as the eluent. Vacuum freeze-drying was performed after three separate backups of the eluent were made. After drying, vacuum-drying, and draining, we removed the salt in accordance with the instructions provided with the C18 ZipTips (Millipore).

LC-MS/MS analysis

For LC-MS/MS, we dissolved peptides in mobile phase A (0.1% formic acid (Fluka) and 2% acetonitrile (Thermo Fisher Scientific) and isolated them using the following liquid-phase gradient settings: 0–40 min, 8–22% B (0.1% formic acid and 90% acetonitrile); 40–52 min, 22–32% B; 52–56 min, 32–80% B; and 56–60 min, 80% B. A UHPLC system (EASY-nLC 1200, Thermo Fisher Scientific) was used for isolation. The flow velocity remained constant at 500 nL/min. The peptides were subsequently fed into an NSI ion source and ionized for examination using a Thermo Fisher Scientific's Orbitrap ExplorisTM 480 mass spectrometer. The FAIMS compensation voltage (CV) was set to −45 V and −65 V, and the ion source voltage was set to 2.3 kV. High-resolution Orbitrap detection and analysis of peptide parent ions and their secondary fragments were performed.

The primary mass spectral scanning range was set to 400–1200 m/z with a scan resolution of 60000, and the secondary mass spectral scanning range was set to 110 m/z with a scan resolution of 30000. Notably, the data collection mode was DDA (data-dependent acquisition), which means that the mother ion of the first 15 peptide fragments with the highest signal intensity was selected and successively entered the HCD collision cell, and crushing was performed with 27% crushing energy. We set the automatic gain control (AGC) to 75%, the signal threshold to 2E4 ions/s, the maximum injection duration to 100 ms, and the tandem mass spectrometry dynamic exclusion time to 30 s.[87]

Database search

The severe acute respiratory syndrome coronavirus-2 library in the NCBI database and the *Mus musculus* library in the UniProt database were analyzed with the MaxQuant search engine (v.2.0.3.1), which searches for modified sites, peptides, and proteins based on the respective download dates (Mus musculus from UniProt on 2020-12-14 and severe acute respiratory syndrome coronavirus-2 from NCBI on 2021-05-26). Each spectrum analyzed for the bait and prey proteins. The cleavage enzyme chosen was trypsin/P, and up to four incomplete cleavages were permitted. When a ubiquitinated lysine was found in the initial search, the mass tolerance for the precursor ions was set to 20 ppm, and the mass tolerance for the fragment ions was set to 0.02 Da. The variable modifications were ubiquitination and oxidation of methionine, while the fixed modification was carbamidomethylation of cysteine. The lowest score of the changed peptides was fixed to more than 40, and the FDR was set to less than 1%. According to the reverse bait database assessment, the FDR for ubiquitinated sites was less than 1%.[88,89]

Bioinformatics analysis

We utilized the motif-x algorithm and MoMo (https://meme-suite.org/meme/tools/momo) to investigate the source of amino acid preference on both sides of the modified site.[90] The minimal number of occurrences, the breadth of motifs, and the elimination of peptides with identically sized core sections were all set to 31. Kyoto Encyclopedia of Genes and Genomes (KEGG) pathway enrichment analysis was subsequently performed using the R package ClusterProfiler (v4.2.1).[91] A p value less than 0.05 indicated statistical significance. Using protein annotations from UniProt, it was possible to determine the subcellular locations of the ubiquitinated proteins. In addition, UbiBrowser 2.0 (http://ubibrowser.bioit.cn/ubibrowser_v3/home/index) was used to determine interactions among E3 ubiquitin-protein ligases, DUBs, and substrate proteins.[92,93] Finally, the STRING website version 11.5 (https://string-db.org/) generated protein−protein interaction (PPI) networks among the differentially expressed ubiquitinated proteins in KEGG pathways with a confidence score of 0.7, which was regarded as the greatest confidence. The interaction networks of proteins in KEGG pathways, SARS-CoV-2, E3 ubiquitin-protein ligases and DUBs were visualized using Cytoscape version 3.9.1 (https://cytoscape.org/download.html).

Immunohistochemical staining

Paraffin-embedded brain tissue sections (5 μm in thickness) were deparaffinized three times in xylene for 10 min and then hydrated in an ethanol gradient (100%, 95%, 80% and 70%). Nonspecific peroxidase activity was blocked for 10 min in hydrogen peroxide, and antigen retrieval was performed by heating the sections in 0.01 M citrate buffer. After blocking in 10% goat serum for 1 h, the sections were stained with an anti-USP29 polyclonal antibody (Invitrogen, PA5-104441; dilution ratio: 1:200) and an anti-PHLDA1 polyclonal antibody (Invitrogen, PA5-119776; dilution ratio: 1:200) at 4°C overnight, followed by incubation with HRP-labeled goat anti-rabbit IgG secondary antibodies (Beijing ZSGB Biotechnology, PV9001) for 60 min. Subsequently, the samples were visualized with 3,30-diaminobenzidine tetrahydrochloride (DAB) and counterstained with hematoxylin. Eventually, the sections were counterstained with hematoxylin, dehydrated and observed under a light microscope (images at 40× magnification).

QUANTIFICATION AND STATISTICAL ANALYSIS

To study the response of the host cerebral cortex to SARS-CoV-2 infection, we collected the cerebral cortexes of 3 infected and 3 uninfected female specific-pathogen-free (SPF) K18-*hACE2* mice for proteomic and ubiquitinated proteomic assays.

We initially removed proteins that matched the MaxQuant-derived data with possible contamination and from the reverse database. Only ubiquitinated sites with a localization probability greater than 0.75 (Class I) were retained. The intensity of proteins or ubiquitinated sites present in more than 50% of samples in the control or SARS-CoV-2 infection groups was considered quantifiable. We calculated the *p* value and fold change (FC) to identify proteins containing upregulated and downregulated quantifiable sites (SARS-CoV-2 infection versus control) and construct a volcano plot after dividing the intensity of the quantifiable ubiquitinated sites in each sample by their corresponding median for normalization and filling the missing values with the smallest of the other values. These sites were utilized in subsequent bioinformatics analyses, such as KEGG analysis. To categorize the differentially expressed ubiquitinated sites, we employed Student's t test with a cutoff *p* value of 0.05. The FC was calculated by dividing the mean intensity of the SARS-CoV-2 infection group by the mean of the control group. A ubiquitinated site with a *p* value of 0.05 and an FC greater than 2 was considered to indicate an upregulated site, whereas a *p* value of 0.05 and an FC less than 0.5 suggested a downregulated site. We created relative Venn diagrams and volcano plots using the "Wu Kong" platform (https://www.omicsolution.com/wkomics/main/)[94] and PCA and UpSet diagrams using the BioLadder platform (https://www.bioladder.cn/web/#/pro/index). We used BLAST version 2.13.0 from NCBI to convert a protein from one species into a corresponding protein from another species.